Geometric scaling behaviors of the Fortuin-Kasteleyn Ising model in high dimensions

Sheng Fang ,[1,2] Zongzheng Zhou ,[3,*] and Youjin Deng [1,2,4,†]

[1]*MinJiang Collaborative Center for Theoretical Physics, College of Physics and Electronic Information Engineering, Minjiang University, Fuzhou 350108, China*

[2]*Hefei National Research Center for Physical Sciences at the Microscales, University of Science and Technology of China, Hefei 230026, China*

[3]*ARC Centre of Excellence for Mathematical and Statistical Frontiers (ACEMS), School of Mathematics, Monash University, Clayton, Victoria 3800, Australia*

[4]*Shanghai Research Center for Quantum Sciences, Shanghai 201315, China*

(Received 19 December 2022; accepted 7 March 2023; published 7 April 2023)

Recently, we argued [Chin. Phys. Lett. **39**, 080502 (2022)] that the Ising model simultaneously exhibits two upper critical dimensions ($d_c = 4$, $d_p = 6$) in the Fortuin-Kasteleyn (FK) random-cluster representation. In this paper, we perform a systematic study of the FK Ising model on hypercubic lattices with spatial dimensions d from 5 to 7, and on the complete graph. We provide a detailed data analysis of the critical behaviors of a variety of quantities at and near the critical points. Our results clearly show that many quantities exhibit distinct critical phenomena for $4 < d < 6$ and $d \geqslant 6$, and thus strongly support the argument that 6 is also an upper critical dimension. Moreover, for each studied dimension, we observe the existence of two configuration sectors, two lengthscales, as well as two scaling windows, and thus two sets of critical exponents are needed to describe these behaviors. Our finding enriches the understanding of the critical phenomena in the Ising model.

DOI: 10.1103/PhysRevE.107.044103

I. INTRODUCTION

The Ising model [1] plays a fundamental role in statistical physics and has an important influence on almost every branch of modern physics. The reduced Hamiltonian of the ferromagnetic Ising model without an external field is

$$\mathcal{H} = -K \sum_{\langle ij \rangle} s_i s_j,$$

where $s_i \in \{-1, 1\}$ is the spin on vertex i, and the coupling strength $K > 0$ acts as the inverse of temperature. The summation $\sum_{\langle ij \rangle}$ is over all pairs of adjacent vertices. The Ising model was first proposed by Lenz in 1920 to explain the ferromagnetic phase transition [2], and Ising showed that in one dimension (1D) there is no phase transition happening at any positive temperature [3]. In 1944, the milestone was achieved by Onsager, who obtained the analytical expression of the free energy on the square lattice and discovered a continuous phase transition [4]. The critical point is $K_c = \ln(1 + \sqrt{2})/2$ [5,6] from duality arguments. The critical exponents β and ν, respectively, characterizing the power-law behavior of the spontaneous magnetization and the divergence of the correlation length near the critical point, are exactly known as $\beta = 1/8$ [7] and $\nu = 1$. It has been proven that the Ising model exhibits a continuous phase transition on hypercubic lattices for all $d \geqslant 3$ [8,9]. In 3D, only numerical estimates are available for both critical points and exponents [10–13]. In particular, the conformal bootstrap method [14], originating from high-energy physics, has significantly improved the precision of critical exponents with the correlation-length exponent $\nu = 0.629\,971(4)$ and susceptibility exponent $\gamma = 1.237\,075(10)$. Renormalization-group (RG) theory predicts that $d_c = 4$ is the upper critical dimension for the Ising model, i.e., for $d \geqslant 4$ critical exponents take their mean-field values, e.g., $\beta = 1/2$ and $\nu = 1/2$ [8,15].

Besides the spin representation, the Ising model has a well-known geometric representation, under the framework of the general Q-state random-cluster (RC) model [16] proposed by Fortuin and Kasteleyn (FK) in 1969. Given a graph $G \equiv (V, E)$ with vertex set V and edge set E, the RC model is defined by choosing a spanning subgraph (V, A) with a probability

$$\pi(A) \propto v^{|A|} Q^{k(A)}.$$

Here $|A|$ is the number of edges on A, and $k(A)$ is the number of connected components (clusters) on A. Parameters v and Q are fugacity for edges and clusters. When Q is an integer, the RC model can be mapped to the Potts model [17], of which $(Q, v) = (2, e^{2K} - 1)$ corresponds to the FK Ising model.

For $Q = 1$, the RC model reduces to the bond percolation model [18]. The RC model not only leads to many exact results in 2D, but it also provides a versatile platform to develop highly efficient cluster algorithms, such as the Wolff algorithm [19], the Swendsen-Wang (SW) algorithm [20], the loop-cluster algorithm [21], etc.

It is natural to ask what is the upper critical dimension of the RC model. In the 1970s, it was suggested from RG analysis that for the general RC model, it could be either 4

*eric.zhou@monash.edu

†yjdeng@ustc.edu.cn

or 6, depending on whether or not the ϕ^3 term is taken into account in the field Hamiltonian [22,23].

For percolation ($Q = 1$) and the Ising model ($Q = 2$), it is well known that their upper critical dimensions are $d_p = 6$ [24] and $d_c = 4$, respectively. However, by studying the FK Ising model on the Bethe lattice and complete graph (CG), the authors in Ref. [25] conjectured that 6 is the upper critical dimension of the FK Ising model, rather than 4. The CG is the graph on which all pairs of vertices are adjacent, and both the CG and Bethe lattice can be regarded as the $d \to \infty$ limit of lattices.

Recently, based on a combination of extensive simulations from $d = 4$ to 7, insights from RG theory, rigorous and numerical results on the CG, we argued that the FK Ising model has two upper critical dimensions $d_c = 4$ and $d_p = 6$, depending on which quantities to be considered [26]. We note that, to our knowledge, $d_p = 6$ cannot be seen from quantities in the spin representation. Compared with Ref. [26], the goal of the current paper is to provide a systematic study of various quantities of the FK Ising model on high-dimensional (high-d) tori (lattices with periodic boundary conditions) and present a more detailed data analysis, such that the two-upper-critical-dimension phenomena are clearly demonstrated.

In the field of critical phenomena, the theory describing the asymptotic approach of finite systems to the thermodynamic limit near a continuous phase transition is called finite-size scaling (FSS). Thus, before moving on to our numerical results, let us briefly review some theoretical predictions to the FSS of the Ising model on high-d tori and boxes (lattices with free boundary conditions). The basic hypothesis of FSS is that the correlation length is cut off by the linear system size L, such that the singular part of the free-energy density can be written as

$$f(t,h) = L^{-d}\tilde{f}(tL^{y_t}, hL^{y_h}),$$

where $t = (K_c - K)/K_c$, h is the magnetic scaling field, and the exponents y_t and y_h are, respectively, the thermal and magnetic renormalization exponents. The scaling behaviors of many quantities can be derived accordingly. For example, the susceptibility χ corresponds to the second derivative of f with respect to h, and it scales as $\chi \sim L^{2y_h-d}$ at the critical point $t = 0$ and with zero field $h = 0$. Above $d_c = 4$, the FSS of the Ising model is controlled by a Gaussian fixed point (GFP), which gives $(y_t, y_h) = (2, 1 + d/2)$, that is, for $d \geqslant 4$ one expects $\chi \sim L^2$. However, it was observed that the FSS of χ above 4D depends on the boundary conditions [27–36]. The scaling L^2 was observed on boxes, but on tori it was observed that $\chi \sim L^{d/2}$.

To understand the behavior on tori, one can turn to the CG. The CG can be regarded as the mean-field approximation of models on high-d tori, since both of them are finite, translational-invariant, and have large vertex degrees. However, models on the CG are often more tractable. For the Ising model on the CG with volume V, it is known that $\chi \sim V^{1/2}\widetilde{\chi}(tV^{1/2})$, with $\widetilde{\chi}(\cdot)$ the scaling function. Let $V = L^d$ and use the scaling formula of χ. Then one can see that the CG asymptotics predict two new exponents $(y_t^*, y_h^*) = (d/2, 3d/4)$ for high-d tori. Since spatial distance is not defined on the CG, it is reasonable to believe that spatial fluctuations are controlled by the GFP. In Ref. [35], it is conjectured that one needs both the CG asymptotics and GFP to fully describe the FSS of the Ising model on high-d tori, and the free energy can be explicitly written as

$$f(t,h) = L^{-d}\tilde{f}_0(tL^{y_t}, hL^{y_h}) + L^{-d}\tilde{f}_1(tL^{y_t^*}, hL^{y_h^*}). \quad (1)$$

Predictions from Eq. (1) for various quantities are all consistent with existing numerical results.

Although Eq. (1) can describe very well the high-d-tori FSS of various quantities in the spin representation, the FSS in the geometric representation is still worth investigating, since many geometric quantities have no direct correspondence in the spin representation. Before presenting results for the FK Ising model on the tori, let us first summarize the results known for the $d = \infty$ case, the CG. At the critical point and within the critical window of width $O(V^{-1/2})$, it was proved that the size of the largest cluster $C_1 \sim V^{3/4}$; this again implies that $(y_t^*, y_h^*) = (d/2, 3d/4)$. For the second-largest cluster, it was proved that $C_2 = O(\sqrt{V}\ln V)$ [37]. Moreover, at $K = K_c - aV^{-1/3}$ with $a > 0$, the system is in the percolation scaling window where $C_1, C_2 \sim V^{2/3}$, the same behavior as the two largest clusters in the critical percolation model on the CG [38]. The Fisher exponent τ, which characterizes the power-law decay of the cluster-number density, was conjectured to be $5/2$ in Ref. [25] and confirmed numerically in Ref. [39]. This is also consistent with the τ value for the critical percolation on the CG [40]. Additionally, in Ref. [39], we found that there is a vanishing sector in the whole configuration space in which the scaling behaviors of all clusters follow the CG-percolation asymptotics, such as $C_1 \sim C_2 \sim V^{2/3}$ and $\tau = 5/2$. The probability of such a percolation sector vanishes with the rate of $V^{-1/12}$. The exponent $1/12$ happens to be the difference between the fractal dimensions of the largest cluster in the FK Ising model and the percolation model.

In this work, we present a systematic study to various quantities of the FK Ising model on tori with d ranging from 5 to 7. We provide solid evidence of the existence of two lengthscales, two configuration sectors, and two scaling windows, from which our conjecture that both $d_c = 4$ and $d_p = 6$ are the upper critical dimensions of the FK Ising model is supported. For $d = 4$, since the theoretical prediction for the forms of logarithmic corrections of geometric quantities is incomplete, we leave the 4D case for future work.

Two length scales. We start with the fractal dimensions of clusters to demonstrate the existence of two lengthscales. Two finite-size fractal dimensions d_{L1}, d_{L2} and two thermodynamic fractal dimensions d_{F1}, d_{F2} are defined via $C_1 \sim L^{d_{L1}} \sim R_1^{d_{F1}}$ and $C_2 \sim L^{d_{L2}} \sim R_2^{d_{F2}}$. Here, R_1 and R_2 are the *unwrapped* radii of gyration for C_1 and C_2, respectively, which represent the radii of the torus that clusters would have on the infinite lattice. Our conjectured values for these fractal dimensions are summarized in Table I, and they are all consistent with numerical estimates. We find that d_{L1} is consistent with $y_h^* = 3d/4$ for $d > 4$, following the CG asymptotics, and d_{L2} is consistent with $1 + d/2$, following the GFP predictions (possibly with multiplicative logarithmic corrections), which recovers the same leading behavior as the CG asymptotics ($V^{1/2}$) in the $d \to \infty$ limit. These results demonstrate that 4 is an upper critical dimension, which is well-known in the spin

TABLE I. Conjectured values and numerical estimates for the finite-size ($d_{\mathrm{L1}}, d_{\mathrm{L2}}$) and thermodynamic ($d_{\mathrm{F1}}, d_{\mathrm{F2}}$) fractal dimensions for the largest and second-largest clusters. The theoretical values are $(d_{\mathrm{L1}}, d_{\mathrm{L2}}) = (3d/4, 1 + d/2)$ for any $d \geqslant 4$, and $(d_{\mathrm{F1}}, d_{\mathrm{F2}}) = (d_{\mathrm{L1}}, d_{\mathrm{L2}})$ for $6 > d \geqslant 4$ and $(9/2, 4)$ for $d \geqslant 6$.

d	5		6		7	
d_{L1}	15/4	3.74(2)	9/2	4.51(1)	21/4	5.18(2)
d_{F1}	15/4	3.76(1)	9/2	4.6(1)	9/2	4.55(12)
d_{L2}	7/2	3.486(11)	4	3.95(7)	9/2	4.48(3)
d_{F2}	7/2	3.61(3)	4	4.0(1)	4	4.1(1)

representation, while for d_{F1} and d_{F2}, we find that they are consistent with d_{L1} and d_{L2} for $d < 6$. However, for $d \geqslant 6$, we find that d_{F1} is consistent with 9/2, and d_{F2} is consistent with 4, independent of the spatial dimensions. We note that 4 is the fractal dimension of percolation clusters on high-d lattices [41]. These results suggest that 6 is another upper critical dimension for the FK Ising model.

From these fractal dimensions, one can easily obtain the scaling behavior of the radius of gyration. For $d < 6$, both R_1 and R_2 are of order $O(L)$. For $d \geqslant 6$, we have $R_1 \sim L^{d_{\mathrm{L1}}/d_{\mathrm{F1}}} = L^{d/6}$, consistent with that of the percolation model [42], and $R_2 \sim L^{d_{\mathrm{L2}}/d_{\mathrm{F2}}} = L^{1/4+d/8}$, both of which are larger than L. Therefore, the topology of these clusters changes at $d_p = 6$, namely, large clusters hardly wind around the torus when $d < 6$ but wind extensively when $d > 6$.

We next move to discuss the behavior of other clusters. Our data show that for other clusters, their sizes s scale with the radii R as $s \sim R^{y_h}$ with $y_h = 1 + d/2$ for $4 < d < 6$ but $s \sim R^4$ for $d \geqslant 6$; the latter is the behavior of percolation clusters on lattices with $d \geqslant 6$. The other interesting quantity to study is the cluster-number density $n(s)$ of these clusters, defined based on the fact that the number of clusters with size in $[s, s + \mathrm{d}s)$ is $L^d n(s)\mathrm{d}s$. It is typically expected that $n(s) \sim s^{-\tau}$ with a cutoff at s close to the size of the largest cluster, and the hyperscaling relation $\tau = 1 + d/d_{\mathrm{L1}}$ is believed to hold. This has been generally observed for percolation models in various dimensions [43] and the FK Ising model below the upper critical dimension [12]. For $d > d_c$, since C_1 is much larger than C_2 and other clusters, it is plausible that the above scaling relation for τ fails. Indeed, for $4 < d < 6$, our numerics suggest that the Fisher exponent $\tau = 1 + \frac{d}{y_h}$ follows the GFP prediction. For $d \geqslant 6$, our data show that $\tau = 5/2$, which is consistent with the percolation model in high dimensions. Thus, the properties of other clusters in the FK Ising model follow the GFP prediction for $4 < d < 6$, but exhibit percolation-cluster behavior for $d \geqslant 6$.

From the fractal dimensions of other clusters and the cluster-number density, one can obtain the scaling of the number of spanning clusters N_s. A cluster is called spanning if its unwrapped extension (defined in Sec. II) exceeds the system size L. From the above discussions, one can see that the two largest clusters are spanning when $d > 6$. For other clusters, we have $s \sim R^4$ above 6D, and thus a cluster is spanning if its size is larger than $O(L^4)$. It then follows that $N_s \sim L^d \int_{L^4} n(s)\mathrm{d}s \sim L^{d-6}$. Thus, N_s is divergent when $d > 6$ and possibly diverges logarithmically at $d = 6$. We note that the scaling behaviors of N_s for $d \geqslant 6$ are the same as in the percolation model [44,45]. By a similar argument, one can obtain that $N_s \sim O(1)$ for $d < 6$. The above scaling for N_s is confirmed by our numerical data.

Two configuration sectors. We then present evidence for the existence of two configuration sectors based on the size distribution of the largest cluster in the critical FK Ising model. Our data indicate that the distribution from finite-size systems converges to the limiting case quite slowly, i.e., a strong finite-size effect. Further investigation reveals that this is due to the existence of a special sector in the whole configuration space. Here, the sector is a set of bond configurations satisfying certain conditions; see Sec. III A 2 for precise definitions. Interestingly, when conditioned on being in this sector, various quantities are observed to follow the GFP prediction for $4 < d < 6$; for example, $C_1, C_2 \sim L^{1+d/2}$. For $d \geqslant 6$, quantities in this sector follow the high-d percolation behavior, like $C_1, C_2 \sim L^{2d/3}$. For all $d > 4$, the weight of the sector vanishes in the limit $L \to \infty$. Numerically, we observed that the vanishing rate is consistent with $L^{1-d/4}$ for $d < d_p$ and $L^{-d/12}$ for $d \geqslant d_p$; the latter is the same as on the CG [39]. We note that for all $d > 4$, the vanishing rate is equal to the difference between the finite-size fractal dimension of the largest cluster in the sector and in the whole configuration space.

Two scaling windows. Finally, we present the existence of the two scaling windows near the critical point. For $d > d_c$, our data show that there is a critical window with a width of order $O(L^{-d/2})$, consistent with the CG prediction that $y_t^* = d/2$. Namely, the FK Ising model at K, where $|K - K_c| = O(L^{-d/2})$ exhibits the same scaling behavior as at the critical point K_c. Moreover, in the high-T regime, our data indicate the existence of another scaling window. For $d = 5$, when $(K - K_c)L^2$ is constant, various quantities follow the GFP prediction, such that $C_1, C_2 \sim L^{1+d/2}$ and the radii R_1, R_2 are of constant order. For $d \geqslant 6$, we find that there is a percolation scaling window with a width of order $O(L^{-d/3})$, i.e., when $(K - K_c)L^{d/3}$ is a constant, the FK clusters behave like percolation clusters. For example, one can observe $C_1, C_2 \sim L^{2d/3}$ and $R_1, R_2 \sim L^{d/6}$.

We then study the thermodynamic behavior of the two radii R_1 and R_2, which involve two correlation-length exponents ν_1 and ν_2 via $R_1 \sim |t|^{-\nu_1}$ as $t \to 0^+$ and $R_2 \sim |t|^{-\nu_2}$ as $t \to 0$. Based on the assumption of the standard FSS, one can recover the thermodynamic behavior from the FSS near K_c. As the critical point is approached from the high-T side ($t \to 0^+$), we find that $\nu_1 = \nu_2 = 1/2$ for all $d > 4$, consistent with the mean-field value for the correlation-length exponent. However, as $t \to 0^-$, we conjecture that $\nu_2 = 2/d$ for $4 < d < 6$ but $\nu_2 = 1/4 + 1/(2d)$ for $d \geqslant 6$. We note that in the $d \to \infty$ limit, one obtains $\nu_2 = 1/4$, which is consistent with the observation on the Bethe lattice [25].

Finally, we note that these abundant phenomena of the FK Ising model cannot be observed within the spin representation. One possible reason is that many quantities in the geometric representation have no direct analog in the spin representation. Under the geometric representation, many spin quantities are decomposed into more refined geometric quantities, which exhibit deeper and more complex properties. For example, the susceptibility in the spin representation becomes the second

TABLE II. The critical points K_c and the largest simulated system volume $V_{\max}$ for $d = 5, 6, 7$ and the CG. For each system, no fewer than N_{sam} independent samples are generated.

d	K_c	$V_{\max}$	N_{sam}
5	0.113 915 0(4) [46]	51^5	5×10^5
6	0.092 298 2(3) [47]	32^6	2×10^5
7	0.077 708 6(8) [47]	20^7	7×10^4
CG	$1/V$	2^{22}	5×10^6

moments of sizes of all clusters in the geometric representation, and obviously the latter contain much richer information. Indeed, by studying the behavior of these cluster, we found out that $d_p = 6$ is another upper critical dimension, i.e., clusters show many distinct behaviors below and above six dimensions.

The remainder of this article is organized as follows. In Sec. II, we provide the details of simulations and sampled quantities. Our numerical results are presented in Secs. III and IV. Finally, we conclude with a discussion in Sec. V.

II. SIMULATION AND OBSERVABLE

We simulate the FK Ising model using a combination of the SW algorithm [20] and the Wolff algorithm [19]. We use the SW algorithm to generate the FK cluster configuration, and between the consecutive SW steps we use the Wolff algorithm to update the spin configurations, since it is believed that the Wolff algorithm has a smaller dynamic exponent than the SW algorithm. We simulate the FK Ising model on high-d tori with $d = 5, 6, 7$ and the CG. The critical points K_c, the largest system volume $V_{\max}$, and the number of independent samples N_{sam} are summarized in Table II. In simulations, we sampled the following observables.

(i) The size of the largest cluster $\mathcal{C}_1$ and the second-largest cluster $\mathcal{C}_2$.

(ii) The number of clusters $\mathcal{N}(s)$ with size in the range $[s, s + \Delta s)$.

(iii) For a cluster C, its radius of gyration $\mathcal{R}(C)$ is defined as

$$\mathcal{R}(C) = \sqrt{\sum_{u\in C} \frac{(\mathbf{x}_u - \bar{\mathbf{x}})^2}{|C|}},$$

where $\bar{\mathbf{x}} = \sum_{u\in C} \mathbf{x}_u/|C|$. Here $\mathbf{x}_u \in \mathbb{Z}^d$ is defined algorithmically as follows. First, choose the vertex, say o, in C with the smallest vertex label according to some fixed but arbitrary labeling. Set $x_o = 0$. Start from the vertex o, and search through the cluster C using breadth-first growth. Iteratively we set $\mathbf{x}_v = \mathbf{x}_u + \mathbf{e}_i$ if the vertex v is traversed from u along the ith direction, and we set $\mathbf{x}_v = \mathbf{x}_u - \mathbf{e}_i$ if it is against the ith direction. Here $\mathbf{e}_i$ is the unit vector in the ith direction. The radii of the largest and second-largest clusters are denoted as $\mathcal{R}_1$ and $\mathcal{R}_2$, respectively.

(iv) The average radius of gyration of clusters with size in $[s, s + \Delta s)$,

$$\mathcal{R}(s) = \frac{\sum_{C:|C|\in[s+\Delta s)} \mathcal{R}(C)}{\mathcal{N}(s)}.$$

(v) For each cluster C, we measure its unwrapped extension $\mathcal{U}$, which is the largest unwrapped distance in the first coordinate direction, i.e., $\mathcal{U} = \max_{u,v\in C}(\mathbf{x}_u - \mathbf{x}_v)_1$.

(vi) The number of spanning clusters $\mathcal{N}_s$. A cluster is spanning if its $\mathcal{U} \geqslant L$.

We choose Δs properly to guarantee there are enough data for statistics in each interval. By taking the ensemble average $\langle\cdot\rangle$ of these observables, we calculate the following quantities:

(i) The mean size of the largest cluster $C_1 = \langle\mathcal{C}_1\rangle$ and the second-largest cluster $C_2 = \langle\mathcal{C}_2\rangle$.

(ii) The radius of gyration $R(s) = \langle\mathcal{R}(s)\rangle$ with a given cluster size s.

(iii) The radius of gyration of the largest and second-largest clusters $R_1 = \langle\mathcal{R}_1\rangle$ and $R_2 = \langle\mathcal{R}_2\rangle$.

(iv) The cluster-number density $n(s, V) = \frac{1}{V\Delta s}\langle\mathcal{N}(s)\rangle$.

(v) The number of spanning clusters $N_s = \langle\mathcal{N}_s\rangle$.

III. RESULTS AT CRITICALITY

We perform least-squares fits on the FSS data. As a precaution against correction-to-scaling terms that we missed including in the fitting ansatz, we impose a lower cutoff $L \geqslant L_{\text{m}}$ on the data points admitted in the fit, and we systematically study the effect on the residual χ^2 value by increasing L_{m}. In general, the preferred fit for any given ansatz corresponds to the smallest L_{m} for which the goodness of fit is reasonable and for which subsequent increases in L_{m} do not cause the χ^2 value to drop by vastly more than one unit per degree of freedom. In practice, by reasonable we mean that $\chi^2/\text{DF} \approx 1$, where DF is the number of degrees of freedom. The systematic error is estimated by comparing estimates from various sensible fitting ansatz.

For quantities without logarithmic corrections, we perform the least-squares fits via the ansatz

$$O = L^{y_O}(a_0 + b_1 L^{y_1} + b_2 L^{y_2}) + c_0. \tag{2}$$

For quantities with logarithmic corrections, we perform the least-squares fits via the ansatz

$$O = L^{y_O}(\ln L + d_0)^{\hat{y}_O}(a_0 + b_1 L^{y_1} + b_2 L^{y_2}) + c_0. \tag{3}$$

Here, we note that $a_0 L^{y_O}$ describes the leading behavior of the quantities, $(\ln L + d_0)^{\hat{y}_O}$ describes the logarithmic corrections, $b_1 L^{y_1}$ and $b_2 L^{y_2}$ describe the finite-size corrections with exponents y_1, y_2 less than 0, and c_0 originates from the background contributions of various systems.

A. Existence of two sectors

1. The probability distribution of the largest cluster

In this section, we consider the probability distribution of the largest cluster $f_{\mathcal{C}_1}(s)$. Define $X_1 = \frac{\mathcal{C}_1}{aV^{3/4}}$ with a constant a and its probability density function as $f_{X_1}(x)$. Then it follows that

$$f_{\mathcal{C}_1}(s)ds = f_{X_1}(x)dx, \tag{4}$$

where $dx = a^{-1}V^{-3/4}ds$ and $f_{X_1}(x) = aV^{3/4} f_{\mathcal{C}_1}(s)$.

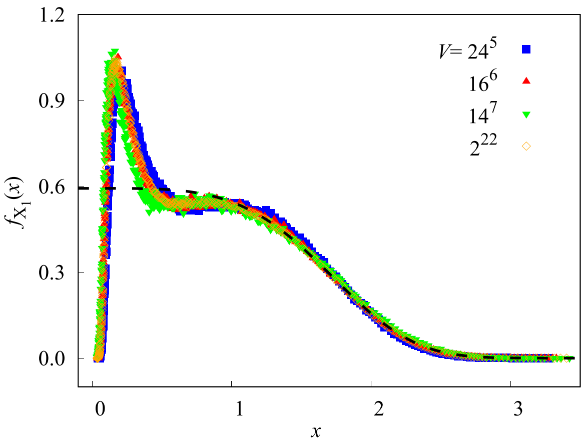

FIG. 1. Probability density functions of the rescaled size of the largest cluster $X_1 := \mathcal{C}_1/aV^{3/4}$. The factor a is chosen to be 1.34, 1.25, 1.06, 1 for $d = 5, 6, 7$ and the CG, respectively. The dashed curve in the plot corresponds to Eq. (5), which is the $V \to \infty$ limiting case. As shown, results on finite-size systems are consistent with the limiting case only when $x \gtrsim 1$. The inconsistency part for small x is due to the existence of an asymptotically vanishing sector in the configuration space, in which the scaling of $\mathcal{C}_1$ is not $V^{3/4}$.

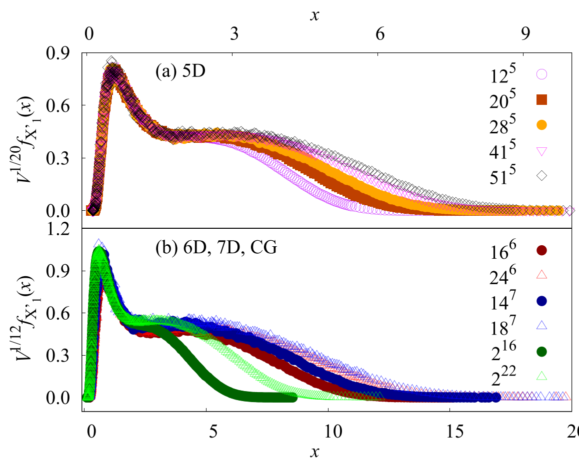

FIG. 2. Demonstration of the vanishing sector, by plotting the probability density functions of the rescaled $\mathcal{C}_1$ for (a) $d = 5$ with $X_1' = \mathcal{C}_1/L^{1+d/2}$ and (b) $d = 6, 7$, and CG with $X_1' = \mathcal{C}_1/V^{2/3}$. This strongly suggests that the sectors vanish with rate $V^{-1/20}$ for 5D and $V^{-1/12}$ for $d \geqslant 6$, and in the sectors the scaling of C_1 is, respectively, $L^{1+d/2}$ and $V^{2/3}$.

On the CG, it was proved in Ref. [37] that the probability density of X_1 with $a = 1$ in the $V \to \infty$ limit follows,

$$f_{X_1}^{\infty}(x) = \frac{\exp(-x^4/12)}{\int_0^{\infty} \exp(-t^4/12)dt}. \tag{5}$$

Later, the authors in Ref. [39] confirmed it numerically. They further found that in finite volume V, the whole configuration space contains a percolation sector in which all clusters exhibit the same scaling behavior as the critical percolation on the CG. The probability of the percolation sector vanishes at a rate of order $V^{-1/12}$.

For $d > d_c = 4$, it is believed that the scaling behavior of the FK Ising model obeys the CG asymptotics. In the study on 5D tori, Lundow *et al.* [48] found that the probability distribution of FK clusters follows the CG asymptotics. In Fig. 1, we plot the probability distribution of the largest cluster $f_{X_1}(x)$ on high-d tori and CG. Similar to CG, it also has a double-peak distribution, and the first peak seems to disappear as system volume increases. We adjust the constant a for various systems so that they have a good data collapse for $x \gtrsim 1$. The dashed line shows the CG prediction Eq. (5). This provides strong evidence that 4 is an upper critical dimension, since for $d > 4$ it exhibits the same asymptotic scaling behavior as in the $V \to \infty$ limit.

We then consider the scaling behavior of the probability density function when $\mathcal{C}_1$ is small. On the CG, a vanishing percolation sector was numerically observed when $\mathcal{C}_1$ is small, and all clusters follow the CG-percolation asymptotics in this sector [39]. For high-d tori, one possible conjecture is that the scaling behavior of the vanishing sector should be consistent with CG for $d > 4$. However, it may bring a problem that $d = 5$ is not sufficient to present the mean-field scaling behavior for percolation since its upper critical dimension is 6. In Ref. [34], it was numerically observed that except for the largest clusters, all other clusters follow the GFP asymptotics. Therefore, we assume that the vanishing sector may follow the GFP asymptotics. Then, we define $X_1' = \mathcal{C}_1/L^{1+d/2}$ for $d = 5$. Figure 2(a) plots $V^{1/20} f_{X_1'}(x)$ versus x, and it is clearly observed that it has a good data collapse for $x \lesssim 3$. We note that the term $V^{1/20} = L^{d/4-1}$ in 5D is from the quotient of the CG-Ising asymptotics $L^{3d/4}$ and the GFP asymptotics $L^{1+d/2}$.

For $d \geqslant 6$, following the same procedure as $d = 5$, we find that the data cannot be well collapsed. We then define $X_1' = \mathcal{C}_1/V^{2/3}$ and Fig. 2(b) shows the plot of $V^{1/12} f_{X_1'}(x)$ against x on high-d tori with $d = 6, 7$ and CG. It can be numerically observed that when x is small, the data collapse well for various systems. Here, we note that the exponent $1/12$ simply originates from the difference between the CG-Ising exponent $3/4$ and the CG-percolation exponent $2/3$. The good data collapse in Fig. 2 implies that there is a vanishing sector. The scaling of $\mathcal{C}_1$ in the sector, i.e., $L^{1+d/2}$ for $d = 5$ and $V^{2/3}$ for $d \geqslant 6$, gives a hint that 6 is also an upper critical dimension.

2. The vanishing sector

We then consider the vanishing rate and scaling behavior of clusters in the vanishing sector. The good data collapse in Fig. 2 implies that there is an exponent θ and positive constants a_0, c_0 so that

$$\lim_{L\to\infty} V^{\theta} \mathbb{P}\left[\frac{\mathcal{C}_1}{V_{\mathrm{van}}} \leqslant a_0\right] = c_0 \tag{6}$$

with $c_0 = \int_0^{a_0} f_{X_1'}(x)dx$. To precisely estimate the exponent θ, we set $a_0 = 1$ and choose $V_{\mathrm{van}} = L^{1+d/2}$ for $d = 5$ and $V_{\mathrm{van}} = V^{2/3}$ for $d \geqslant 6$, and we count the probability P of configurations with the size of the largest cluster $\mathcal{C}_1 \in (0, V_{\mathrm{van}}]$. We then perform the least-squares fits via the ansatz Eq. (2) with L substituted by V. The final estimates of θ are 0.046(4) for $d = 5$ and 0.088(3), 0.087(9) for $d = 6, 7$, respectively; the former for $d = 5$ is consistent with the expected value 1/20, and the latter for $d = 6, 7$ is consistent with 1/12

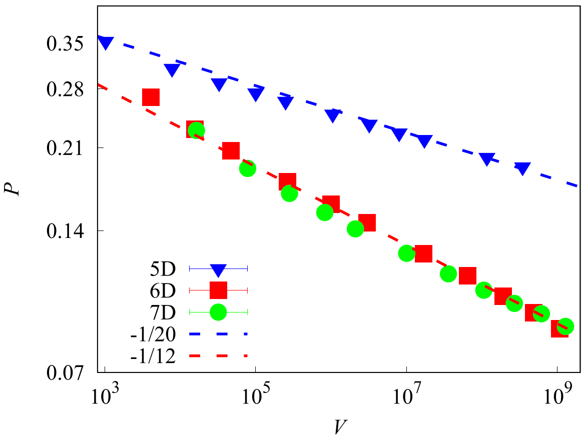

FIG. 3. Plot to show that the vanishing rate of the vanishing sector is $V^{-1/20}$ for 5D and $V^{-1/12}$ for $d = 6, 7$. For $d \geqslant 6$, the rate is consistent with the observation on the CG.

within two standard deviations. Figure 3 presents the probability P versus system volume V in the log-log scale for $d = 5, 6, 7$, and the slopes of the data are well consistent with their expected value. We define the vanishing sector as the set of configurations with $\mathcal{C}_1 \leqslant V_{\rm van}$. In this sector, it can be implied that the largest cluster $C_1 \sim L^{1+d/2}$ for $d = 5$ and $C_1 \sim L^{2d/3}$ for $d = 6, 7$. We then consider the probability density of the second-largest cluster $\mathcal{C}_2$. We define the variable $X_2' = \mathcal{C}_2/L^{1+d/2}$ for $d = 5$ and $X_2' = \mathcal{C}_2/(aV^{2/3})$ for $d = 6, 7$ and CG. Figure 4(a) shows $f_{X_2'}(x)$ against x, and the good data collapse suggests that $C_2 \sim L^{1+d/2}$, following the GFP asymptotics. Figure 4(b) implies $C_2 \sim V^{2/3}$ for $d = 6, 7$ and CG. The data from 6D and 7D collapse well, but there is a little discrepancy with CG, which may originate from the choice of constant a_0. The different scaling behaviors of the vanishing sectors imply 6 is a special dimension, which gives another hint for geometric upper critical dimension $d_p = 6$.

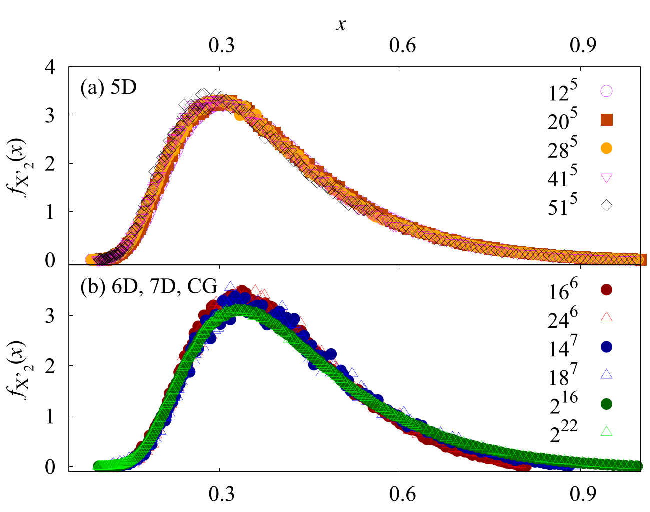

FIG. 4. The probability density function of the rescaled second-largest cluster in the vanishing sector, which displays different scaling behaviors for (a) $d = 5$ and (b) $d = 6, 7$ and CG. The variable $X_2' := \mathcal{C}_2/L^{1+d/2}$ for $d = 5$ and $X_2' := \mathcal{C}_2/(aV^{2/3})$ with $a = 1.23, 1.12, 1$ for $d = 6, 7$, and CG, respectively.

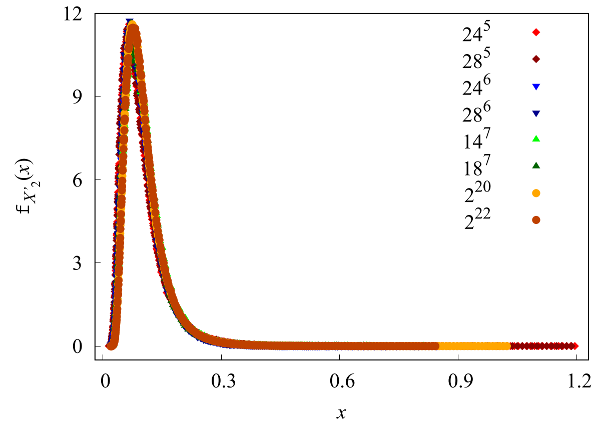

FIG. 5. The probability density function of the rescaled second-largest cluster in the Ising sector. The variable $X_2' := \mathcal{C}_2 \ln L/(aL^{1+d/2})$ with $a = 4.70, 4.22, 4.67$ for $d = 5, 6, 7$, respectively, and $X_2' := \mathcal{C}_2/(V^{1/2}\ln V)$ for CG.

3. Ising sector

Except for the vanishing sector, we also define the Ising sector, whose probability approaches 1 as system volume goes to infinity. To suffer from less finite-size corrections, we include only the configurations with $\mathcal{C}_1 \geqslant V^{3/4}$ to the Ising sector. In this sector, its largest cluster follows the CG asymptotics $C_1 \sim V^{3/4}$. For the second-largest cluster $\mathcal{C}_2$, we define $X_2' = \mathcal{C}_2 \ln L/(aL^{1+d/2})$ for high-d tori and $X_2' = \mathcal{C}_2/(V^{1/2}\ln V)$ for CG, and the data can collapse well for various systems, as shown in Fig. 5.

B. Existence of the two-lengthscale behavior

1. Finite-size fractal dimensions $d_{\rm L1}$ and $d_{\rm L2}$

In this section, we study the two-lengthscale behavior by extracting the finite-size fractal dimensions $d_{\rm L1}$ and $d_{\rm L2}$. We first recall the theoretical study on the CG. In Ref. [37], it was numerically observed that the critical FK Ising model on the CG has two-lengthscale behavior, in which the largest cluster $C_1 \sim V^{3/4}$ and the second-largest cluster $C_2 \sim O(V^{1/2}\ln V)$ have different scaling behaviors, which was further numerically testified in Ref. [39]. Later, numerical results on the 5D FK Ising model also showed its two-lengthscale behavior [34].

In a previous study [34], we argued that the scaling behaviors of the FK Ising model on the 5D tori are simultaneously governed by the CG asymptotics and the GFP asymptotics, which were supported by large-scale Monte Carlo simulation results. Based on it, we argue that the largest cluster $C_1 \sim L^{3d/4}$ and the second-largest cluster $C_2 \sim L^{1+d/2}/\ln L$, which gradually converges to the CG scaling behavior $V^{1/2}\ln V$ in the $d \to \infty$. Note that the appearance of the multiplicative logarithmic correction $1/\ln L$ in the scaling of C_2 is conjectured purely according to our numerical data; see below for details. Figure 6 plots C_1 and $\tilde{C}_2 \equiv C_2 \ln L/L$ versus the system volume V, and data from various systems collapse well with slopes consistent with $3/4$ and $1/2$, respectively. To

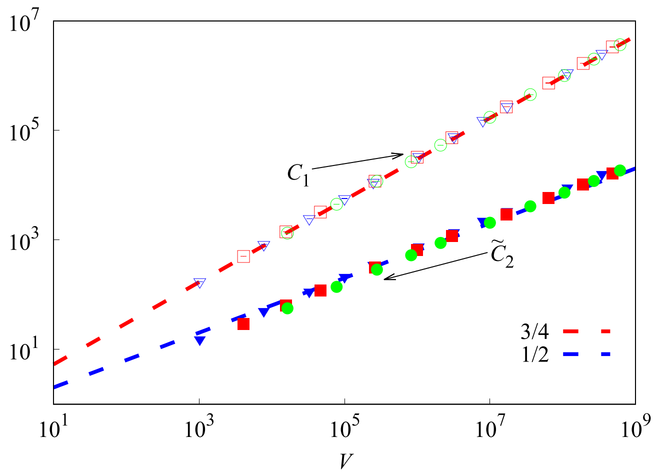

FIG. 6. The FSS behaviors of the largest cluster C_1 (hollow points) and second-largest cluster $\tilde{C}_2 := C_2 \ln L/L$ (solid points) for various system sizes with $d = 5$ (blue), $d = 6$ (red), and $d = 7$ (green). These scaling behaviors follow the CG asymptotics.

extract the value of the finite-size fractal dimensions d_{L1} and d_{L2}, we perform the least-squares fits to the MC data.

We first consider the largest cluster C_1 for $d > 4$. We perform the least-squares fits to it via the ansatz Eq. (2). The fitting results are summarized in Table III. For $d = 5$, we first set $b_2 = c_0 = 0$ and leave other parameters free, and we obtain $d_{L1} = 3.743(2)$ and $y_1 = -1.9(2)$ with $L_m = 8$. Leaving c_0 free also gives a consistent estimate $d_{L1} = 3.736(11)$. By comparing with various ansatz, we finally get the estimate $d_{L1} = 3.74(2)$, which is consistent with the expected value $15/4$. For $d = 6$, we first set $b_2 = 0$ and leave other parameters free, but it does not yield stable results. Consequently, we fix the correction exponent y_1 and obtain the estimates $d_{L1} = 4.510(7)$ for $y_1 = -2$ and $d_{L1} = 4.505(10)$ for $y_1 = -3$. By comparing various ansatz, we obtain the final estimate $d_{L1} = 4.51(1)$, which is consistent with the expected value $9/2$. For $d = 7$, following a similar procedure, we obtain the final estimate $d_{L1} = 5.18(2)$, which is close to the expected value $21/4$. The discrepancy between the estimate and the expected value may be due to the fact that the precision of the critical threshold is not high enough, such that the true critical point is slightly away from the quoted value in Ref. [47].

TABLE III. Estimates of the finite-size fractal dimension d_{L1} with $d \geqslant 5$ via ansatz Eq. (2). The conjectured values of d_{L1} are $15/4$, $9/2$, $21/4$ for $d = 5, 6, 7$, respectively.

d	L_m	d_{L1}	a_0	b_1	y_1	χ^2/DF
	6	3.743(2)	1.160(7)	−1.1(3)	−1.9(2)	4.4/6
5	8	3.743(3)	1.16(1)	−1(1)	−2.1(6)	4.3/5
	6	4.508(4)	1.00(1)	0.5(3)	−2	1.7/5
	8	4.510(7)	1.00(2)	0.8(9)	−2	1.6/4
6	6	4.506(3)	1.009(9)	3(2)	−3	1.8/5
	8	4.509(6)	1.00(2)	8(9)	−3	1.5/4
	10	4.505(9)	1.01(3)	−5(26)	−3	1.3/3
	5	5.196(5)	1.12(2)	−12(2)	−3	6.4/6
	6	5.188(8)	1.14(3)	−17(5)	−3	4.9/5
7	7	5.18(1)	1.18(5)	−28(13)	−3	4.2/4
	4	5.190(4)	1.14(1)	−2.0(1)	−2	6.6/7
	5	5.183(7)	1.16(2)	−2.5(4)	−2	5.0/6
	6	5.18(1)	1.19(4)	−3.1(9)	−2	4.3/5

TABLE IV. Estimates of the finite-size fractal dimension d_{L2} for $d \geqslant 5$ with multiplicative logarithmic corrections via the ansatz Eq. (3). The conjectured values of d_{L2} are $7/2$, 4, $9/2$ for $d = 5, 6, 7$, respectively.

d	L_m	d_{L2}	$\hat{y}_O$	a_0	b_1	y_1	χ^2/DF
	10	7/2	−1.05(1)	1.09(2)	−1.25(4)	−1/2	1.9/5
	12	7/2	−1.06(2)	1.11(3)	−1.29(6)	−1/2	1.2/4
	16	7/2	−1.08(3)	1.15(6)	−1.4(1)	−1/2	0.6/3
5	10	3.490(2)	−1	1.06(1)	−1.19(2)	−1/2	1.5/5
	12	3.489(3)	−1	1.07(1)	−1.20(3)	−1/2	1.1/4
	16	3.485(6)	−1	1.09(3)	−1.25(7)	−1/2	0.7/3
	8	4	−0.99(3)	0.94(3)	−17(2)	−2	7.7/4
	10	4	−1.07(5)	1.05(6)	−26(5)	−2	2.9/3
	12	4	−1.3(2)	1.3(3)	−59(33)	−2	1.5/2
6	8	4.003(7)	−1	0.94(2)	−17(1)	−2	7.8/4
	10	3.98(1)	−1	1.02(4)	−25(4)	−2	2.9/3
	12	3.94(4)	−1	1.2(2)	−47(22)	−2	1.5/2
	7	4.49(1)	−1	1.64(7)	−1.9(1)	−1/2	2.7/5
	8	4.48(2)	−1	1.7(1)	−2.0(2)	−1/2	2.5/4
7	7	9/2	−1.04(4)	1.7(1)	−2.0(2)	−1/2	2.7/5
	8	9/2	−1.06(7)	1.7(2)	−2.1(3)	−1/2	2.4/4

We then consider the second-largest cluster C_2. We assume that it scales as $C_2 \sim L^{1+d/2}/\ln L$ for $d \geqslant 5$. We perform the least-squares fits to it via the ansatz Eq. (3). Taking $d = 5$ as an example, leaving y_O and $\hat{y}_O$ free cannot yield reasonable results. We then fix $y_O = 7/2$ and obtain the estimate $\hat{y}_O = -1.07(6)$. We then fix $\hat{y}_O = -1$ and obtain $y_O = 3.49(1)$, which is consistent with the expected value $7/2$. Following a similar procedure, we obtain the estimates $d_{L2} = 3.95(7), 4.48(3)$ for $d = 6, 7$, respectively, and the logarithmic correction exponents are consistent with -1. These estimates are consistent with our conjecture $C_2 \sim L^{1+d/2}/\ln L$, and the fitting results are summarized in Table IV.

In addition, we also try to fit the C_2 data to the ansatz Eq. (2) without logarithmic corrections. We obtain the estimates $d_{L2} = 3.32(1), 3.71(3), 4.32(2)$ for $d = 5, 6, 7$, respectively. These estimates all deviate away from the expected values. This is why we believe there exists the logarithmic correction $1/\ln L$ in the scaling behavior of C_2.

2. *Thermodynamic fractal dimensions d_{F1} and d_{F2}*

We then consider the thermodynamic fractal dimensions d_{F1} and d_{F2}. To extract their values, we plot the largest cluster C_1 versus its radius R_1 and the second-largest cluster C_2 versus its radius R_2 in the log-log scale, as seen in Fig. 7. The slopes of lines indicate the fractal dimensions. We find that d_{F1} is consistent with the finite-size fractal dimension $d_{L1} = 3d/4$ for $4 < d < 6$, while for $d \geqslant 6$ it is consistent with $9/2$, independent of the spatial dimension. For the fractal dimension

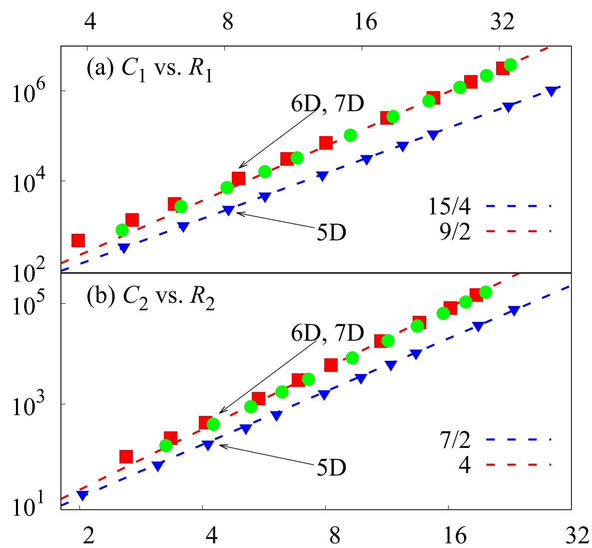

FIG. 7. The log-log plot of (a) the largest cluster C_1 vs its radius R_1 and (b) the second-largest cluster C_2 vs its radius R_2 for various system sizes in $d = 5$ (blue), $d = 6$ (red), and $d = 7$ (green).

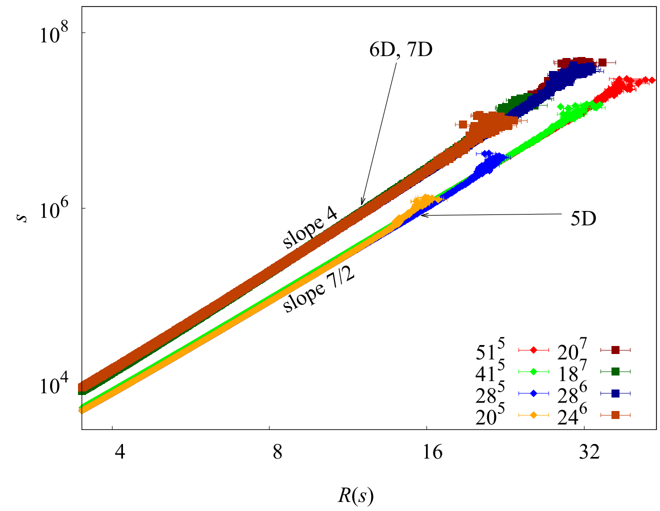

FIG. 8. The log-log plot of the clusters size s vs their radius $R(s)$ for $d \geqslant 5$. The slopes display the thermodynamic fractal dimension $D_{\rm F}$.

$d_{\rm F2}$, we find that it is consistent with $1 + d/2$ for $4 < d < 6$ and 4 for $d \geqslant 6$.

We then perform the least-squares fits to the MC data. For $d \geqslant 5$, we assume C_1 and C_2 do not require logarithmic correction, and we take the fitting ansatz Eq. (2). The results are summarized in Table V. Considering the systematic error from various fitting ansatz, we finally estimate $d_{\rm F1} = 3.76(1), 4.6(1), 4.55(12)$ and $d_{\rm F2} = 3.61(3), 4.0(1), 4.1(1)$ for $d = 5, 6, 7$, respectively. Except for $d_{\rm F2}$ in $d = 5$, all of these estimates are consistent with our conjecture. The slight disagreement of the estimate of $d_{\rm F2}$ to its expected value at 5D might be due to the potential logarithmic corrections.

We next study the thermodynamic fractal dimension for clusters other than C_1 and C_2. We plot the size of these clusters s versus their radius R for $d \geqslant 5$ in Fig. 8. In the log-log plot, the slopes of lines indicate the value of $d_{\rm F2}$, and we find for all critical clusters with medium size that the fractal dimension is consistent with $d_{\rm F2}$. As Fig. 8 shows, we find for $d = 5$ that the slope of the line is consistent with $1 + d/2$, following the GFP asymptotics, while for $d \geqslant d_p$ it has a good data collapse with a slope consistent with 4, which has the same value as the high-d percolation model.

To summarize, for $d > 4$, the two-lengthscale behavior begins to appear with the finite-size fractal dimensions $d_{\rm L1} = 3d/4$ and $d_{\rm L2} = 1 + d/2$, consistent with the CG asymptotics. For $d \geqslant 6$, the thermodynamic fractal dimensions $d_{\rm F1}$, $d_{\rm F2}$ are no longer the same as the finite-size fractal dimensions and consistent with dimension-independent constants 9/2 and 4, respectively. The two-lengthscale behavior of the fractal dimensions gives solid support for the simultaneous existence of the two upper critical dimensions.

TABLE V. Estimates of the thermodynamic fractal dimensions $d_{\rm F1}$ and $d_{\rm F2}$ with $d = 5, 6, 7$. The exponent y_O corresponds to $d_{\rm F1}$ for C_1 and $d_{\rm F2}$ for C_2 in each dimension.

d	O	$L_{\rm m}$	y_O	a_0	b_1	c_0	y_1	χ^2/DF
	C_1	6	3.768(4)	2.25(3)	3(2)	7(9)	−1.8(3)	2.0/5
5		8	3.767(6)	2.27(5)	6(11)	−10(58)	−2(1)	1.6/4
	C_2	6	3.620(3)	2.38(3)	6(2)	3(4)	−2.3(2)	1.7/5
		8	3.616(4)	2.40(3)	27(50)	−35(65)	−2.9(7)	1.0/4
		6	4.56(6)	0.36(9)	3.0(1)		−1.05(3)	6.1/4
	C_1	4	4.59(3)	0.30(3)	2.71(1)	24(1)	−1	6.5/6
6		5	4.58(3)	0.32(4)	2.707(8)	26(2)	−1	5.4/5
	C_2	4	3.95(2)	1.58(9)	3.9(5)	3(2)	−1.7(2)	2.5/5
		5	4.03(5)	1.2(3)	2.5(2)	−10(2)	−1.0(2)	1.0/4
		6	4.58(4)	0.6(1)	3.1(6)		−1.3(2)	2.9/5
7	C_1	7	4.55(6)	0.7(2)	4(3)		−1.5(5)	2.7/4
		5	4.08(3)	1.4(1)	3.8(6)		−1.6(2)	5.1/6
	C_2	6	4.06(4)	1.5(2)	5(2)		−1.8(2)	4.9/5

3. Scaling behavior of radius R_1 and R_2

From the scaling behaviors $C_1 \sim L^{d_{\rm L1}} \sim R_1^{d_{\rm F1}}$ and $C_2 \sim L^{d_{\rm L2}} \sim R_2^{d_{\rm F2}}$, we have $R_1 \sim L^{d_{\rm L1}/d_{\rm F1}}$ and $R_2 \sim L^{d_{\rm L2}/d_{\rm F2}}$. Thus, the scaling behaviors of R_1 and R_2 follow,

$$\begin{aligned} &R_1 \sim R_2 \sim L, && d \leqslant 6, \\ &R_1 \sim L^{d/6}, \quad R_2 \sim L^{1/4+d/8}, && d > 6. \end{aligned} \tag{7}$$

Note that we ignore the logarithmic corrections for R_2.

We first consider R_1 and plot R_1/L versus L for various systems, as shown in Fig. 9. For $4 < d < 6$, as system size increases, we find that R_1/L converges to a constant for $4 < d < 6$ but increases for $d \geqslant 6$. This means the largest cluster does not wind around the torus below 6D but winds extensively above 6D. To verify the precise scaling behavior of R_1, we perform the least-squares fits to MC data via the ansatz Eq. (2), where O corresponds to R_1 and y_O corresponds to $d_{\rm R1}$. The fitting results are summarized in Table VI. We find for $d \leqslant 6$ that $d_{\rm R1}$ is consistent with 1, while it is larger than 1 for $d = 7$. Nevertheless, it is not consistent with 7/6, which may be due to the fact that the precision of the critical threshold is not high enough.

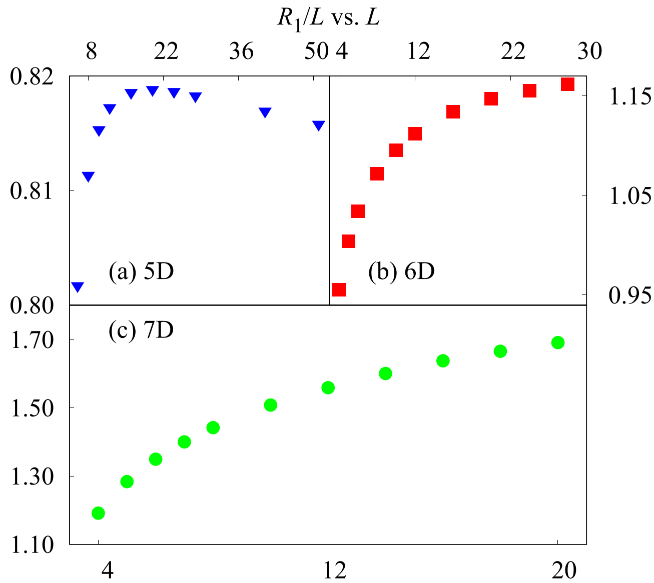

FIG. 9. The FSS behavior of the rescaled radius R_1/L vs system size L for (a) $d = 5$, (b) $d = 6$, and (c) $d = 7$. For $d < d_p$, the radius R_1 is bounded by the linear system size L, while it increases faster than L for $d > d_p$.

We then consider R_2. In Fig. 10, we plot the rescaled radius R_2/L versus its system size L. As L increases, R_2/L converges to a constant for $d \leqslant 6$, but it increases for $d = 7$.

4. Cluster number density $n(s, L)$

We then consider the cluster-number density $n(s, L)$. Generally, it is expected that

$$n(s, L) \sim s^{-\tau}\tilde{n}(s/L^{d_{L1}}), \tag{8}$$

where τ is the Fisher exponent. The universal scaling function $\tilde{n}(x)$ is approximately a constant for $x \ll 1$ and drops quickly for $x \gg 1$. The exponents τ and d_{L1} are not independent but obey the hyperscaling relation

$$\tau = 1 + d/d_{L1}. \tag{9}$$

The above scaling behavior of $n(s, L)$ has been observed for percolation models in various dimensions and random-cluster models below $d_c = 4$ [12].

TABLE VI. The fitting results of the radius of the largest cluster R_1 for $d = 5, 6, 7$. For $d \leqslant 6$, it is of order L, while it deviates from L for $d > 6$.

d	L_m	d_{R1}	a_0	b_1	b_2	y_1	y_2	χ^2/DF
5	8	0.999(2)	0.809(9)	0.17(3)	−0.61(5)	−2/3	−4/3	2.6/5
	10	0.997(3)	0.82(1)	0.11(6)	−0.5(1)	−2/3	−4/3	1.5/4
6	10	1.001(2)	1.19(1)	−1.01(4)		−1		4.0/3
	12	0.997(4)	1.21(2)	−1.10(7)		−1		1.8/2
	6	1.102(7)	1.30(4)	−1.2(2)	0.5(5)	−1	−2	6.7/5
	7	1.09(1)	1.35(7)	−1.4(5)	1(1)	−1	−2	6.2/4
7	6	1.08(2)	1.44(10)	−0.9(3)	−0.2(4)	−2/3	−4/3	6.5/5
	7	1.07(3)	1.5(2)	−1.3(7)	0.4(9)	−2/3	−4/3	6.0/4

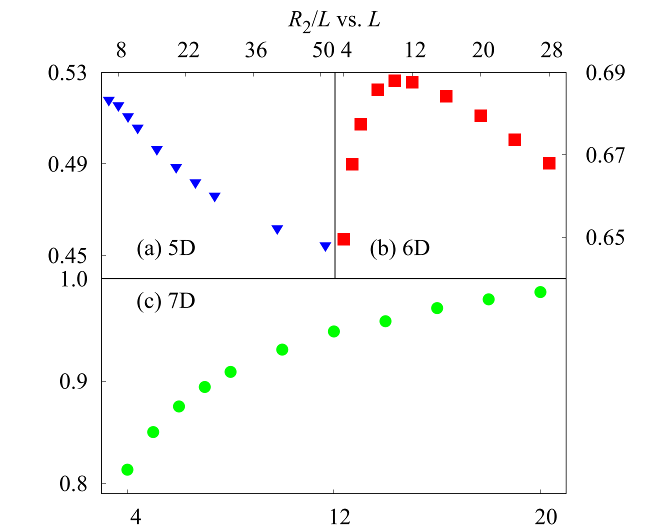

FIG. 10. The FSS behavior of the rescaled radius R_2/L vs system size L for (a) $d = 5$, (b) $d = 6$, and (c) $d = 7$. For $d \leqslant d_p = 6$, the radius R_2 is bounded by the linear system size L, while it increases faster than L for $d > d_p$.

We then plot $n(s, L)$ versus cluster size s for $5 \leqslant d \leqslant 7$, shown in Fig. 11. As we can see, it first displays a power-law behavior with the slope being the Fisher exponent τ, then it enters a plateau, and finally it decays significantly. Our data show that τ is consistent with 17/7 for $d = 5$ and 5/2 for $d = 6, 7$; the latter was conjectured in Ref. [25] and is consistent with the value of the FK Ising model on the CG [39] and the percolation model on high-d tori and the CG [43]. Thus, it supports $d_p = 6$ is an upper critical dimension.

We note that, using the values of d_{L1} in Table I, the scaling relation Eq. (9) is broken. Using these values of τ, one can obtain an effective fractal dimension d_{eff} using Eq. (9). For $d = 5$, since $\tau = 17/7$, one has $d_{\text{eff}} = 7/2$, consistent with $d_{L2} = 1 + d/2$ from the GFP prediction. For $d \geqslant 6$, using $\tau = 5/2$, one has $d_{\text{eff}} = 2d/3$, which is the fractal dimension of the percolation clusters on high-d tori and CG.

5. Number of spanning cluster N_s

We next study the number of spanning clusters N_s. Recall that a cluster is spanning if its unwrapped distance $\mathcal{U}$ is not less than the linear size L. We plot N_s versus L for $d = 5, 6, 7$ in Fig. 12. For $d < 6$, we see N_s converges to a bounded value, while for $d \geqslant 6$, N_s increases as the system size increases. For $d = 6$, the straight line in the semilog plot in Fig. 12(b) suggests $N_s \sim \ln L$, and the straight line in the log-log plot with a slope close to 1 in Fig. 12(c) suggests $N_s \sim L$ for $d = 7$, which is consistent with the observation on the high-d percolation [42].

The divergence of N_s above 6D can be understood from the behavior of $n(s, L)$. As discussed in Sec. III B 2, for clusters except the largest one, their sizes scale with the radius of gyration as $s \sim R^4$ for $d \geqslant 6$. It is reasonable to expect the unwrapped distance $\mathcal{U}$ of a cluster is of the same order as R. Thus, it follows that a spanning cluster has R no less than L, and thus its size s is at least of order L^4. Thus, the number of

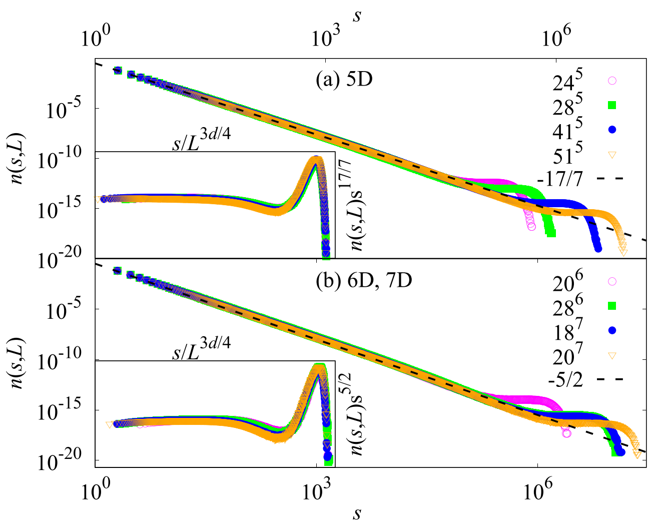

FIG. 11. The cluster-number density $n(s, L)$ for (a) $d = 5$ and (b) $d = 6, 7$. The Fisher exponent τ is consistent with $1 + \frac{d}{1+d/2}$ for $d < d_p$ and 5/2 for $d \geqslant d_p$.

spanning clusters above 6D can be calculated as

$$N_s \sim L^d \int_{L^4}^{L^d} n(s, L)\mathrm{d}s \sim L^{d-6}.$$

So N_s diverges as L^{d-6} for $d > 6$, which is the same as the percolation model on high-d tori [44]. In the marginal case $d = 6$, possibly N_s diverges logarithmically.

To verify the scaling of N_s, we perform the least-squares fits to the MC data. For $d = 6$, we use the logarithmic fitting ansatz Eq. (3) with $y_O = 0$. We first leave $\hat{y}_O$ free, but no stable results can be obtained. We then fix $\hat{y}_O = 1$, $y_1 = -1$, and leave a_0, b_1, c_0 free, and we obtain stable fits when $L_\mathrm{m} = 16$, which gives $a_0 = 19(2)$, $b_1 = -150(20)$, and $c_0 = 23(9)$ with the residuals $\chi^2 \approx 0.9$. For $d = 7$, we fit the MC data to the ansatz Eq. (2). We first set $b_1 = b_2 = 0$ and leave a_0, c_0, and y_O free, which gives unstable results. Leaving the correction exponent y_1 or y_2 free cannot yield stable results. Thus, we fix the exponent y_1 to various values, and we leave a_0, b_1, c_0, and y_O free. The fitting results are summarized in Table VII.

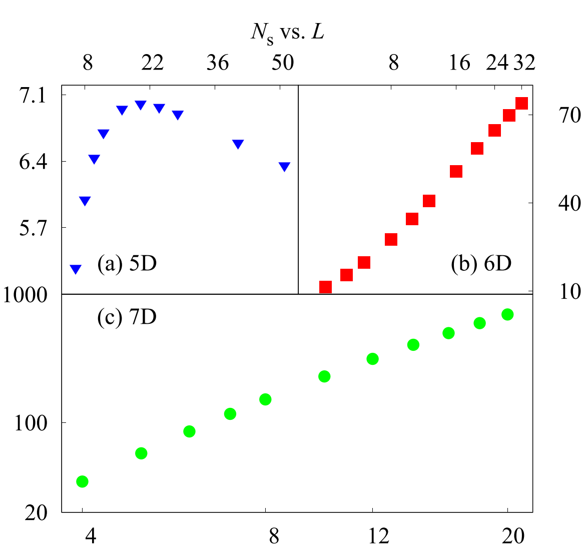

FIG. 12. The number of spanning clusters N_s, which is bounded for (a) $d = 5$ and diverges for $d = 6$ and 7. The semilog plot in (b) implies $N_s \sim \ln L$ for $d = 6$. The log-log plot in (c) implies N_s for $d = 7$ diverges as a power law.

TABLE VII. The fitting results of the number of spanning cluster N_s for $d = 7$, which is consistent with the conjecture $N_s \sim L$.

d	L_m	y_O	a_0	b_1	c_0	y_1	χ^2/DF
7	7	0.97(1)	90(6)	−292(27)	250(27)	−1/2	1.5/4
	8	0.99(3)	80(11)	−244(52)	201(53)	−1/2	0.5/3

IV. RESULTS NEAR CRITICALITY

In this section, we consider the critical behavior away from the critical point K_c. We study the coupling strength $K = K_c - aL^{-\lambda}$ with $\lambda > 0$, i.e., the reduced temperature $t = \frac{1}{K_c}aL^{-\lambda}$. When $a > 0$, the critical point $t = 0$ is approached from the high-T side, and $a < 0$ is from the low-T side. We study the scaling behavior for different values of λ. For $d > d_c$, we find there are asymmetric behaviors as K_c is approached from different sides, and the asymmetric behaviors are different for $4 < d < 6$ and $d \geqslant 6$. On the high-T side, we find that there exists more than one scaling window.

A. High-temperature side

We recall some scaling behaviors that are believed to hold near criticality. First, for $d \geqslant 4$, the leading FSS behavior of the magnetic susceptibility χ reads

$$\chi(t, L) \simeq L^{2y_h^*-d}\tilde{\chi}(tL^{y_t^*}) = L^{d/2}\tilde{\chi}(tL^{d/2}), \tag{10}$$

where the RG exponents $(y_h^*, y_t^*) = (3d/4, d/2)$ from the CG asymptotics have been used. In the thermodynamic limit $(L \to \infty)$, χ exhibits singular scaling behavior as $\chi(t) \sim t^{-\gamma}$, and the mean-field value $\gamma = 1$ can be obtained either from the GFP or the CG asymptotics. We ask how the FSS ansatz (10) transits to the thermodynamic scaling. Given any infinitesimal but finite t, the argument $x \equiv tL^{d/2}$ in the function $\tilde{\chi}(x)$ would diverge for sufficiently large L. To eliminate the explicit dependence of L, it is requested that $\tilde{\chi}(x) \sim x^{-1}$ for $x \gg 1$. Therefore, if the Ising critical point is approached from the high-T side as $t \sim L^{-\lambda}$ with $\lambda < d/2$, one has $\chi \sim L^\lambda$. Indeed, it was numerically observed [32] that χ on high-d tori follows,

$$\chi \sim \begin{cases} L^\lambda & \text{if } \lambda < d/2, \\ L^{d/2} & \text{if } \lambda \geqslant d/2. \end{cases} \tag{11}$$

For $\lambda \geqslant d/2$, since the renormalized scaling field $tL^{d/2}$ in Eq. (10) does not flow away, the FSS behaviors of all the quantities, including χ, should be the same as those at the critical point, as presented in Sec. III.

Second, for $0 < \lambda < d/2$, the cluster-number density $n(s, L)$ should obey a similar form to Eq. (8). Taking into account the potential two lengthscales, we separate the contribution from the largest cluster and write

$$n(s, L) \sim s^{-\tau}\tilde{n}(s/s_\lambda) + L^{-d}f_{C_1}(s, L). \tag{12}$$

The factor L^{-d} is for the density of the largest cluster, which might have a λ-dependent fractal dimension $d_{\lambda 1}$, and $f_{\mathcal{C}_1}(s, L)$ denotes the cluster-size distribution of the largest cluster. For $4 \leqslant d < 6$, the Fisher exponent is $\tau = 1 + d/d_{\mathrm{F}}$ with $d_{\mathrm{F}} = 1 + d/2$ from the GFP. Further, if the cutoff size $s_\lambda \sim L^{d_\lambda}$, the number of clusters of size $O(s_\lambda)$ would diverge as $N_\lambda \sim L^{d(1-d_\lambda/d_{\mathrm{F}})}$ for $d_\lambda < d_{\mathrm{F}}$. For $d \geqslant 6$, one has $\tau = 5/2$, and N_λ is divergent for $d_\lambda < 2d/3$.

Since the magnetic susceptibility is identical to the second moment of cluster sizes as $\chi = \sum_s s^2 n(s, L)$, we have

$$\chi \sim (s_\lambda)^{3-\tau} + bL^{2d_{\lambda 1}-d}, \tag{13}$$

where b is a positive constant. Depending on the value of λ, the leading scaling behavior of χ might come from the largest cluster, from the remaining ones, or equally from both.

Third, as the temperature decreases, the correlation length ξ, corresponding to the diameters of characteristic clusters, grows as $\xi \sim t^{-\nu}$, with $\nu = \nu_g = 1/2$ from the GFP. For $t \sim L^{-\lambda}$, one would have $\xi \sim L^{\lambda/2}$, suggesting that $\lambda = \lambda_g = 2$ is a special value. For $\lambda < \lambda_g$, the diameters of clusters are much smaller than the linear size L. For $\lambda > \lambda_g$, the correlation length ξ might be restricted to be of order L or it might increase faster than L. In this case, finite-size effects become important.

Fourth, it is helpful to consider the two-point correlation function $g(r, L)$, which is the probability for two vertices with distance r to be in the same cluster. By definition, the susceptibility is $\chi \equiv \sum g(r, L)$, where the translational invariance on the tori is used. For $\lambda < \lambda_g = 2$, we expect $g(r) \sim r^{2-d}\tilde{g}(r/\xi)$, where $\xi \ll L$, and $\tilde{g}(x)$ drops exponentially for $x \gg 1$. For $\lambda > 2$, $g(r, L)$ develops a plateau for large distance due to finite-size effects, which would contribute to the leading scaling behavior of χ. According to Eq. (11), one has

$$g(r, L) \sim \begin{cases} r^{2-d}\,\tilde{g}(r/L^{\lambda/2}) & \text{if } \lambda \in (0,\ 2), \\ r^{2-d} + O(L^{\lambda-d}) & \text{if } \lambda \in [2,\ d/2), \\ r^{2-d} + O(L^{-d/2}) & \text{if } \lambda \in [d/2,\ \infty). \end{cases} \tag{14}$$

Thus, for $\lambda > 2$, $g(r, L)$ exhibits the crossover behavior from the power-law decay, as predicted by GFP, to a distance-independent plateau. The crossover happens at $r = O(L^{(\lambda-d)/(2-d)})$ for $2 < \lambda \leqslant d/2$ and at $r = O(L^{d/2(d-2)})$ for $\lambda > d/2$. The summation over the r-dependent part of the correlation function $g(r, L)$ gives $\chi \sim L^\lambda$ for $\lambda \leqslant 2$, and $\chi \sim L^2$ for $\lambda > 2$, serving only as the subleading behavior of χ. To verify this scenario, one can define the magnetic structure factor as $\chi_{\mathbf{k}} \equiv \sum g(\mathbf{r}) \exp(i\mathbf{k} \cdot \mathbf{r})$ and take the lowest momentum $|\mathbf{k}| = 2\pi/L$. Since the Fourier transformation would eliminate the contribution from the plateau of $g(r, L)$, one expects $\chi_{\mathbf{k}} \sim L^2$ for $\lambda \geqslant 2$, which was indeed observed in the previous studies [29,30,32].

1. 4 < *d* < 6

For $\lambda < 2$, the critical point is approached at such a low speed that the diameters of the large clusters, though diverging, are much smaller than the linear size L. Finite-size effects are negligible, and the critical behaviors of the medium-size clusters are governed by the GFP. Namely, one has the cluster size $s \sim R^{d_g}$ with $d_g \equiv 1 + d/2$ for radii $1 \ll R \ll L^{\lambda/2}$, and the cutoff size is $s_\lambda \sim L^{\lambda d_g/2}$. In Eq. (13), the contribution to χ from the largest cluster is of order $O(L^{\lambda-d(1-\lambda/2)}) < O(L^\lambda)$, and thus the FSS of χ is from the summation over all the clusters. Actually, since the number N_λ of large clusters of characteristic size s_λ is $N_\lambda \sim L^{d(1-\lambda/2)}$, the contribution from these large clusters is already of order $O(L^\lambda)$.

For $\lambda = \lambda_g = 2$, corresponding to the so-called Gaussian scaling window of width $O(L^{-2})$, the correlation length ξ reaches the order of L. There are only finite characteristic clusters $N_\lambda \sim O(1)$; a plateau of height L^{2-d} develops in the scaling of the correlation function $g(r, L)$ for large r.

For $\lambda \geqslant d/2$, i.e., the CG-Ising scaling window, the results in Sec. III show that the unwrapped diameters of the largest and second-largest clusters are $R_1 \sim R_2 \sim L$. Two lengthscales are exhibited in the sizes of clusters: the largest cluster scales as $C_1 \sim L^{3d/4}$, and all the other clusters have the Gaussian fractal dimension $d_g = 1 + d/2$. The leading FSS $\chi \sim L^{d/2}$ is merely from the largest cluster, or equivalently, from the plateau of $g(r, L)$.

For $\lambda_g < \lambda < d/2$, one naturally expects that $R_1 \sim R_2 \sim L$ and the Gaussian fractal dimension holds true for all clusters except C_1. Further, from the leading FSS behavior $\chi \sim L^\lambda$, one obtains $d_{\mathrm{F}1} = d_{\mathrm{L}1} = (d + \lambda)/2$ for the largest cluster.

2. *d* ⩾ 6

The scaling behaviors for $\lambda \leqslant 2$ should be similar to those for $4 \leqslant d < 6$, except that the Gaussian fractal dimension $d_{\mathrm{F}} = d_g$ should be replaced by $d_{\mathrm{F}} = 4$, which can be regarded as being from branching random walks. Namely, for medium-size clusters with radii $1 \ll R \ll \xi$, one has $s \sim R^4$, which is independent of d.

For $\lambda > 2$, we first consider $\lambda = \lambda_p = d/3$, corresponding to the CG-percolation scaling window of width $O(L^{-\lambda_p})$, and we expect that the FK-Ising clusters exhibit nearly the same geometric properties as those in the standard bond percolation model on high-d tori. The unwrapped correlation length grows faster than L as $\xi_u \sim L^{\lambda/2} = L^{d/6}$. All the clusters, including C_1, scale as $s \sim R_u^4$ until the cutoff size $s_\lambda \sim \xi_u^4 \sim L^{2d/3}$. The Fisher exponent is $\tau = 5/2$, and the number of clusters of cutoff sizes is $O(1)$. In other words, as the standard percolation clusters in high dimensions, the FK-Ising clusters manage to keep their shape to be "thin" by avoiding touching each other and wrapping around the tori for a diverging number of times ($\xi_u/L = L^{d/6-1}$). This is indicated by Figs. 8, 7, and 12(c) and other plots in Sec. III. It is interesting to note that, in terms of the unwrapped distance r_u, the two-point correlation function decays as Gaussian-like as $g(r, L) \sim r_u^{2-d}$ until the unwrapped correlation length, giving $\chi \sim \xi_u^2 \sim L^{d/3}$ [31,33]. The situations for $\lambda_g < \lambda < \lambda_p$ are similar to those for the percolation scaling window. We have $\xi_u \sim L^{\lambda/2}$, $s_\lambda \sim \xi_u^4 \sim L^{2\lambda}$, and $\chi \sim \xi_u^2 \sim L^\lambda$.

For $\lambda \in (d/3, d/2)$, we argue that the scaling of the unwrapped diameter of the largest cluster becomes λ-independent as $R_1 \sim L^{d/6}$, as for $\lambda = \lambda_p$ and $\lambda \geqslant d/2$. Meanwhile, C_1 becomes "fat" by merging the second-largest and other clusters, and, from the FSS of χ, we have $C_1 \sim L^{d_{\mathrm{L}1}} \sim R_1^{d_{\mathrm{F}1}}$, with $d_{\mathrm{L}1} = (d + \lambda)/2$ and $d_{\mathrm{F}1} = 4 + \delta_\lambda$, where $\delta_\lambda \equiv \lambda/\lambda_p - 1$ is introduced.

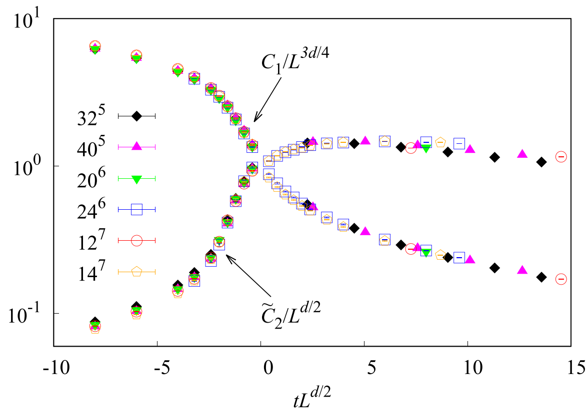

FIG. 13. The CG-Ising scaling window illustrated by the rescaled cluster sizes $C_1/L^{3d/4}$ and $\tilde{C}_2/L^{d/2} = C_2 \ln L/L^{1+d/2}$ on high-d tori with $d = 5, 6, 7$. Both C_1 and C_2 follow the CG asymptotics.

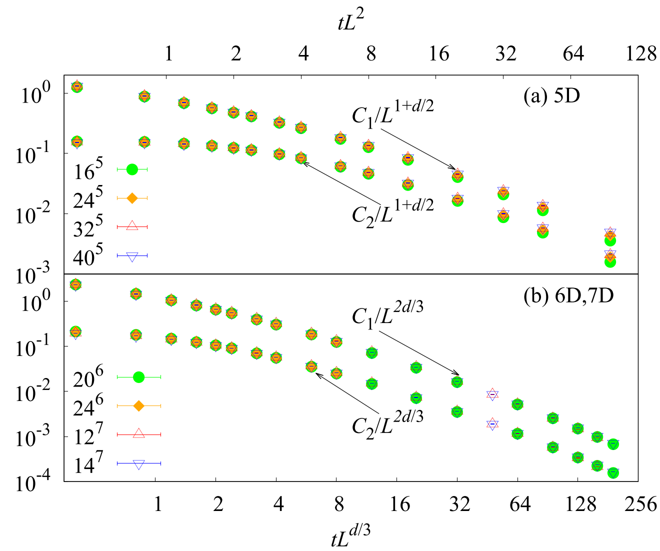

FIG. 14. The Gaussian and CG-percolation scaling windows illustrated by C_1 and C_2 on high-d tori with (a) $d = 5$ and (b) $d = 6, 7$.

We expect that all the medium-sized clusters scale as $s \sim R^4$ until the cutoff size s_λ. Since all clusters with $s > s_\lambda$ are merged into the largest cluster, s_λ should decrease as λ increases. For the second-largest cluster C_2, by assuming a linear interpolation between $d_{L2} = 2d/3$ for $\lambda = \lambda_p$ and $d_{L2} = 1 + d/2$ for $\lambda = d/2$, we obtain the finite-size fractal dimension $d_{L2} = (d - \lambda) + 2\delta_\lambda$. With the assumption $C_2 \sim R_2^4$, we have $R_2 \sim L^{d_{L2}/4}$, which is also divergent for $d > 6$. An argument for $d_{L2} \geqslant d - \lambda$ can be provided as follows. As λ increases from λ_p, all the clusters larger than $s_\lambda \sim C_2 \sim L^{d_{L2}}$ are merged into the largest cluster, contributing to a total size of $L^d \int_{s_\lambda} sn(s, L)\mathrm{d}s \sim L^{d-d_{L2}/2}$. Thus, we have $L^{d-d_{L2}/2} \leqslant C_1 \sim L^{(d+\lambda)/2}$, giving $d_{L2} \geqslant d - \lambda$. Note that δ_λ is a d-independent constant, and thus the lower bound $d - \lambda$ becomes sharper and sharper as d increases.

In a brief summary, as the critical point is approached as $O(L^{-\lambda})$ from the high-T side, the FK-Ising model exhibits the simultaneous existence of the CG-Ising scaling window of width $O(L^{-d/2})$ and of the Gaussian scaling window of width $O(L^{-2})$. For $d \geqslant 6$, in between, there exists another scaling window of width $O(L^{-d/3})$, corresponding to the CG-percolation scaling window. Since the high-d percolation exhibits both the Gaussian and CG-percolation scaling windows, we say that the FK-Ising model for $d \geqslant 6$ exhibits the simultaneous existence of the high-d percolation and the CG-Ising scaling windows. As λ increases, the correlation length ξ reaches the order of L already in the Gaussian scaling window. For $4 \leqslant d < 6$, $\xi \sim L$ saturates as long as $\lambda > 2$, and the largest and second-largest clusters display different geometric properties. For $d > 6$, the correlation length in an unwrapped way saturates in the high-d percolation scaling window as $\xi_u \sim L^{d/6}$, and the two-lengthscale behaviors develop for $\lambda > d/3$. As an illustration, Figs. 13–15 display the FSS behaviors of the largest and second-largest clusters in the CG-Ising, Gaussian, and CG-percolation scaling windows. Table VIII lists the exact values of critical exponents for different λ and d, including the finite-size and thermodynamic fractal dimensions as well as the scaling exponents for the unwrapped cluster diameters.

B. Low-temperature side

We then consider that the critical point is approached from the low-T side, i.e., $a < 0$. When the temperature is decreased, more and more clusters merge into the largest cluster, such that the second-largest cluster C_2 becomes smaller and smaller. One would not expect to observe the percolation scaling windows with $\lambda = d/3$, in which $C_2 \sim L^{2d/3}$. Recall that it was observed that the Ising model on the CG has a critical window with a width of order $O(V^{-1/2})$ both for the spin representation and FK representation [37,49]. Thus, one would expect that within this critical window, the FSS behaviors are the same as those at criticality. In other words, for $\lambda \in [d/2, \infty)$, the scaling behavior is the same for the

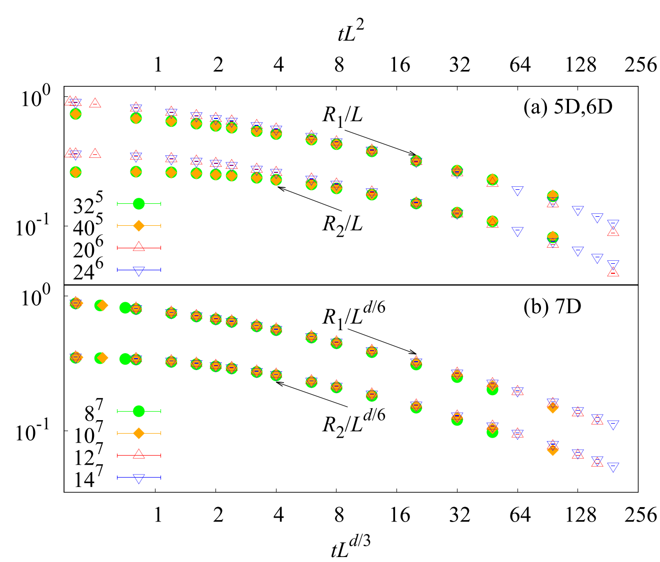

FIG. 15. The Gaussian and CG-percolation scaling windows illustrated by the unwrapped radii R_1 and R_2 on high-d tori with (a) $d = 5, 6$ and (b) $d = 7$.

TABLE VIII. Finite-size and thermodynamic fractal dimensions, $d_{\mathrm{L}i}$ and $d_{\mathrm{F}i}$, for the largest and second-largest clusters ($i = 1, 2$), as the critical point is approached at a speed of $O(L^{-\lambda})$ from the high-temperature side. The unwrapped diameters of clusters scale as $R_i \sim L^{d_{\mathrm{R}i}}$, with $d_{\mathrm{R}i} = d_{\mathrm{L}i}/d_{\mathrm{F}i}$ For clarity, we use $d_g = d/2 + 1$ and $\delta_\lambda = \lambda/\lambda_p - 1$ with $\lambda_p = d/3$. Note that the exact values of many of these exponents are conjectured on the basis of numerics, insights from RG theory and CG asymptotics, or even from linear interpolation.

		Largest cluster			Second-largest cluster		
d	$\lambda \in$	$d_{\mathrm{L}1}$	$d_{\mathrm{F}1}$	$d_{\mathrm{R}1}$	$d_{\mathrm{L}2}$	$d_{\mathrm{F}2}$	$d_{\mathrm{R}2}$
	(0,2)	$\frac{\lambda}{2}d_g$	d_g	$\frac{\lambda}{2}$	$\frac{\lambda}{2}d_g$	d_g	$\frac{\lambda}{2}$
[4,6)	$[2, \frac{d}{2})$	$\frac{\lambda+d}{2}$	$d_{\mathrm{L}1}$	1	d_g	$d_{\mathrm{L}2}$	1
	$[\frac{d}{2}, \infty)$	$\frac{3}{4}d$	$d_{\mathrm{L}1}$	1	d_g	$d_{\mathrm{L}2}$	1
	$(0, \frac{d}{3})$	2λ	4	$\frac{\lambda}{2}$	2λ	4	$\frac{\lambda}{2}$
[6, ∞)	$[\frac{d}{3}, \frac{d}{2})$	$\frac{\lambda+d}{2}$	$4+\delta_\lambda$	$\frac{1}{6}d$	$d-\lambda+2\delta_\lambda$	4	$\frac{1}{4}d_{\mathrm{L}2}$
	$[\frac{d}{2}, \infty)$	$\frac{3}{4}d$	$\frac{9}{2}$	$\frac{1}{6}d$	d_g	4	$\frac{1}{4}d_{\mathrm{L}2}$

high-T approach and low-T approach, and the corresponding exponents are listed in Table VIII. In Fig. 13, we plot the rescaled cluster sizes $C_1/L^{3d/4}$ and $C_2 \ln L/L^{1+d/2}$ versus $tL^{d/2}$. The good data collapse gives solid support to the existence of the critical window.

C. Crossover to the thermodynamic limit

From above, we find there is an asymmetric FSS behavior from the high-T and low-T approaches, which is unconventional in most critical systems. Here, we note that it not only affects the FSS behavior, but also the thermodynamic scaling behavior.

Like the susceptibility χ in Eq. (10), we assume that the FSS scaling behaviors of other quantities obey a similar form to

$$\mathcal{Q}(t, L) = L^{y_{\mathcal{Q}}\lambda_t}\tilde{\mathcal{Q}}(tL^{\lambda_t}). \tag{15}$$

Moreover, under the condition that the quantity $\mathcal{Q}$ is well defined directly in the thermodynamic limit, we assume that the scaling function follows

$$\tilde{\mathcal{Q}}(x) \sim \begin{cases} \text{const}, & x \to 0, \\ |x|^{-y_{\mathcal{Q}}}, & x \to \infty, \end{cases} \tag{16}$$

such that $\mathcal{Q}(t)$ returns to the thermodynamic scaling behavior $\mathcal{Q}(t) \sim |t|^{-y_{\mathcal{Q}}}$. For χ, the exponents $y_{\mathcal{Q}} = \gamma = 1$ and $\lambda_t = d/2$. We then take the radii R_1 and R_2 as an example and consider the correlation-length exponents ν_1 and ν_2, which are defined as $R_1(t) \sim |t|^{-\nu_1}$ and $R_2(t) \sim |t|^{-\nu_2}$. We note that ν_2 can be well defined both from the high-T and low-T sides, while ν_1 is only well defined from the high-T side.

We first consider the high-T approach. We assume that the radii R_1 and R_2 have the same scaling behavior $R_{1,2}(t, L) \sim L\tilde{R}_{1,2}(tL^2)$ for $4 < d < 6$, such that we obtain $\nu_1 = \nu_2 = 1/2$. In this case, it is consistent with the scaling behavior in Table VIII. In other words, if one takes $t \sim L^{-\lambda}$ it turns out to be $R_{1,2} \sim L^{\lambda/2}$ for $\lambda \leqslant \lambda_t = 2$ and $R_{1,2} \sim L$ for $\lambda > \lambda_t$. For $d \geqslant 6$, following a similar procedure, we assume the scaling behaviors $R_{1,2} \sim L^{d/6}\tilde{R}_{1,2}(tL^{d/3})$ and $R_{1,2}(t) \sim |t|^{-1/2}$. Figure 16 illustrates the above thermodynamic scaling behaviors of R_1 and R_2.

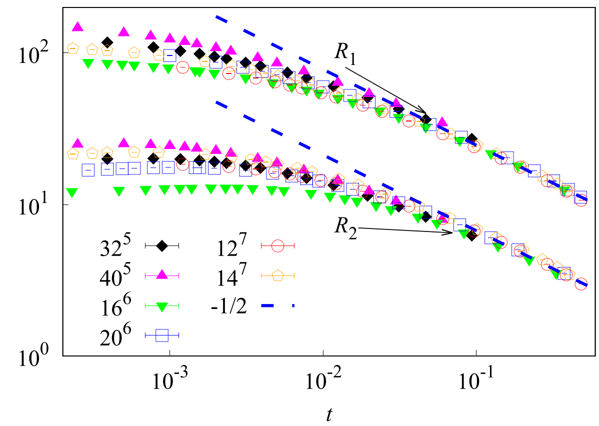

FIG. 16. The thermodynamic scaling behavior of the radius R_1 and R_2 from the high-T approach for $d = 5, 6, 7$.

We then consider that it approaches the critical point from the low-T side. Since one has $R_2 \sim L\tilde{R}_2(tL^{d/2})$ for $4 < d < 6$ and $R_2 \sim L^{1/4+d/8}\tilde{R}_2(tL^{d/2})$ for $d \geqslant 6$, it is expected that $R_2(t) \sim |t|^{-\nu_2}$ with $\nu_2 = 2/d$ for $4 < d < 6$ and $\nu_2 = 1/4 + 1/2d$ for $d \geqslant 6$. As $d \to \infty$, the exponent ν_2 reduces to 1/4, consistent with the calculation on the Bethe lattice [25].

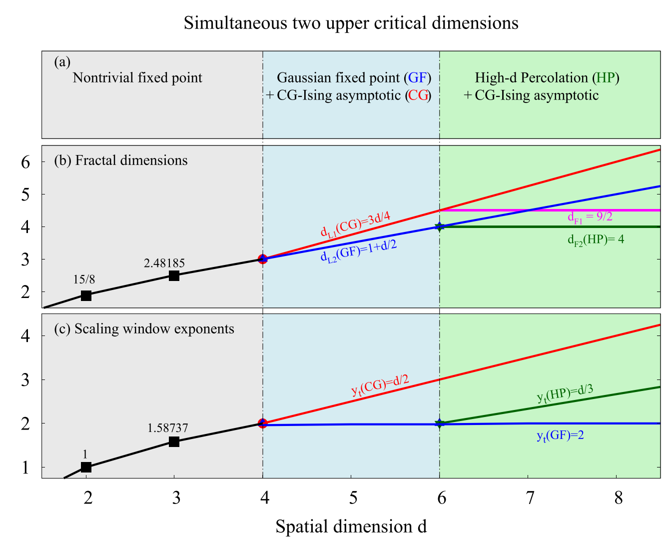

FIG. 17. Demonstration of the simultaneous two upper critical dimensions of the Ising model in its FK representation. The scaling behaviors are governed by nontrivial fixed points for $d < 4$, by the Gaussian fixed point asymptotics and complete graph asymptotics for $4 < d < 6$, and by the complete graph asymptotics and high-d percolation asymptotic for $d \geqslant 6$, as illustrated in (a). The values of the finite-size fractal dimension d_{L} and of the thermodynamic fractal dimension d_{F} are given in (b) for the largest cluster and the second-largest cluster. The value of the thermal-like renormalization exponent y_t, governing the size of the corresponding scaling window as $O(L^{-y_t})$, is given in (c).

V. DISCUSSION

In this work, we perform large-scale Monte Carlo simulations on high-dimensional (high-d) tori and the complete graph (CG). Based on our numerical results, we provide a detailed and complete report to support our conjecture of the simultaneous existence of the two upper critical dimensions ($d_c = 4, d_p = 6$) in the Fortuin-Kasteleyn (FK) representation of the Ising model. Other rich phenomena are further observed. In particular, as long as $d > d_c$, there are two configuration sectors, two-lengthscale behaviors, and two scaling windows. The scaling behaviors are conjectured to be governed by the Gaussian fixed point (GFP) asymptotics and CG-Ising asymptotics for $4 < d < 6$, and by the CG-Ising asymptotics and high-d percolation asymptotics for $d \geqslant 6$. For clarity, the d-dependent values of various critical exponents are summarized in Fig. 17. It is unexpected at first glance that for $d \geqslant d_p$, many scaling behaviors of the FK-Ising clusters are the same as the critical high-d percolation, including the thermodynamic fractal dimension $d_{F2} = 4$ and the scaling behavior of the radius $R_1 \sim L^{d/6}$ and the number of spanning clusters $N_s \sim L^{d-6}$.

The rich phenomena observed in the FK representation deepen our understanding of the Ising model. A natural question is whether these phenomena can be observed in other representations. For the spin representation, critical behaviors are simpler: no percolation-like behaviors exist and the upper critical dimension $d_p = 6$ does not exist. Apart from the FK representation, there is another geometric representation, i.e., the loop representation, which can be linked to the FK representation in the framework of the loop-cluster joint model [21]. Recently, it was shown in Ref. [50] that studying the loop representation on the CG within the framework of the loop-cluster joint model provides a natural and simple explanation for the appearance of percolation behaviors in the FK Ising model, which results in the existence of two lengthscales, two configuration sectors, and two scaling windows. Thus, we would expect that the study of the loop representation on high-dimensional tori, which is still under our investigation, would provide some explanations for the observations in the FK Ising model on tori, especially for the two upper critical dimensions.

Here, we emphasize that the general scenario in Fig. 17 is just a conjecture based on extensive simulations and insights from exact CG solutions and the existing RG calculations. Further studies are needed to judge the validity of the conjectured scenario in Fig. 17 as well as the values of the critical exponents.

ACKNOWLEDGMENTS

This work has been supported by the National Natural Science Foundation of China (under Grant No. 12275263), and the National Key R&D Program of China (under Grant No. 2018YFA0306501). We thank Eren M. Elçi, Jens Grimm, Timothy Garoni, Martin Weigel, Jonathan Machta, and Jesper Jacobsen for valuable discussions.

[1] S. Friedli and Y. Velenik, *Statistical Mechanics of Lattice Systems: A Concrete Mathematical Introduction* (Cambridge University Press, Cambridge, 2017).

[2] W. Lentz, Beitrag zum verständnis der magnetischen erscheinungen in festen Körpern, Z. Phys. **21**, 613 (1920).

[3] E. Ising, Beitrag zur Theorie des Ferromagnetismus, Z. Phys. **31**, 253 (1925).

[4] L. Onsager, Crystal statistics. I. A two-dimensional model with an order-disorder transition, Phys. Rev. **65**, 117 (1944).

[5] H. A. Kramers and G. H. Wannier, Statistics of the two-dimensional ferromagnet. Part I, Phys. Rev. **60**, 252 (1941).

[6] R. Baxter, *Exactly Solved Models in Statistical Mechanics*, Dover Books on Physics (Dover, New York, 2007).

[7] C. N. Yang, The spontaneous magnetization of a two-dimensional Ising model, Phys. Rev. **85**, 808 (1952).

[8] M. Aizenman and R. Fernández, On the critical behavior of the magnetization in high-dimensional Ising models, J. Stat. Phys. **44**, 393 (1986).

[9] M. Aizenman, H. Duminil-Copin, and V. Sidoravicius, Random currents and continuity of Ising models spontaneous magnetization, Commun. Math. Phys. **334**, 719 (2015).

[10] Y. Deng and H. W. J. Blöte, Simultaneous analysis of several models in the three-dimensional Ising universality class, Phys. Rev. E **68**, 036125 (2003).

[11] A. M. Ferrenberg, J. Xu, and D. P. Landau, Pushing the limits of Monte Carlo simulations for the three-dimensional Ising model, Phys. Rev. E **97**, 043301 (2018).

[12] P. Hou, S. Fang, J. Wang, H. Hu, and Y. Deng, Geometric properties of the Fortuin-Kasteleyn representation of the Ising model, Phys. Rev. E **99**, 042150 (2019).

[13] 3D Ising model: The scaling equation of state, Nucl. Phys. B **489**, 626 (1997).

[14] F. Kos, D. Poland, D. Simmons-Duffin, and A. Vichi, Precision islands in the Ising and O(N) models, J. High Energy Phys. 08 (2016) 036.

[15] R. Fernandez, J. Fröhlich, and A. Sokal, *Random Walks, Critical Phenomena, and Triviality in Quantum Field Theory*, Theoretical and Mathematical Physics (Springer, Berlin, 2013).

[16] G. R. Grimmett, *The Random-cluster Model* (Springer Science & Business Media, Berlin, 2006), Vol. 333.

[17] F. Y. Wu, The Potts model, Rev. Mod. Phys. **54**, 235 (1982).

[18] D. Stauffer and A. Aharony, *Introduction to Percolation Theory* (CRC, Boca Raton, FL, 2018).

[19] U. Wolff, Collective Monte Carlo Updating for Spin Systems, Phys. Rev. Lett. **62**, 361 (1989).

[20] R. H. Swendsen and J.-S. Wang, Nonuniversal Critical Dynamics in Monte Carlo Simulations, Phys. Rev. Lett. **58**, 86 (1987).

[21] L. Zhang, M. Michel, E. M. Elçi, and Y. Deng, Loop-Cluster Coupling and Algorithm for Classical Statistical Models, Phys. Rev. Lett. **125**, 200603 (2020).

[22] R. K. P. Zia and D. J. Wallace, Critical behaviour of the continuous n-component Potts model, J. Phys. A **8**, 1495 (1975).

[23] D. J. Amit, Renormalization of the Potts model, J. Phys. A **9**, 1441 (1976).

[24] J. T. Chayes and L. Chayes, On the upper critical dimension of bernoulli percolation, Commun. Math. Phys. **113**, 27 (1987).
[25] L. Chayes, A. Coniglio, J. Machta, and K. Shtengel, Mean-field theory for percolation models of the Ising type, J. Stat. Phys. **94**, 53 (1999).
[26] S. Fang, Z. Zhou, and Y. Deng, Geometric upper critical dimensions of the Ising model, Chin. Phys. Lett. **39**, 080502 (2022).
[27] E. Brézin and J. Zinn-Justin, Finite size effects in phase transitions, Nucl. Phys. B **257**, 867 (1985).
[28] K. Binder, M. Nauenberg, V. Privman, and A. P. Young, Finite-size tests of hyperscaling, Phys. Rev. B **31**, 1498 (1985).
[29] M. Wittmann and A. P. Young, Finite-size scaling above the upper critical dimension, Phys. Rev. E **90**, 062137 (2014).
[30] E. Flores-Sola, B. Berche, R. Kenna, and M. Weigel, Role of Fourier Modes in Finite-Size Scaling above the Upper Critical Dimension, Phys. Rev. Lett. **116**, 115701 (2016).
[31] J. Grimm, E. M. Elçi, Z. Zhou, T. M. Garoni, and Y. Deng, Geometric Explanation of Anomalous Finite-Size Scaling in High Dimensions, Phys. Rev. Lett. **118**, 115701 (2017).
[32] Z. Zhou, J. Grimm, S. Fang, Y. Deng, and T. M. Garoni, Random-Length Random Walks and Finite-Size Scaling in High Dimensions, Phys. Rev. Lett. **121**, 185701 (2018).
[33] J. C. Grimm, Finite-size effects in high dimensional physical systems, Ph.D. thesis, Monash University, Clayton, Victoria, Australia (2018).
[34] S. Fang, J. Grimm, Z. Zhou, and Y. Deng, Complete graph and Gaussian fixed-point asymptotics in the five-dimensional Fortuin-Kasteleyn Ising model with periodic boundaries, Phys. Rev. E **102**, 022125 (2020).
[35] J.-P. Lv, W. Xu, Y. Sun, K. Chen, and Y. Deng, Finite-size scaling of O(n) systems at the upper critical dimensionality, Natl. Sci. Rev. **8**, nwaa212 (2021).
[36] F. Camia, J. Jiang, and C. M. Newman, The effect of free boundary conditions on the ising model in high dimensions, arXiv:2011.02814.
[37] M. Luczak and T. Łuczak, The phase transition in the cluster-scaled model of a random graph, Random Struct. Alg. **28**, 215 (2006).
[38] B. Bollobás, G. Grimmett, and S. Janson, The random-cluster model on the complete graph, Probab. Theor. Relat. Fields **104**, 283 (1996).
[39] S. Fang, Z. Zhou, and Y. Deng, Percolation effects in the Fortuin-Kasteleyn Ising model on the complete graph, Phys. Rev. E **103**, 012102 (2021).
[40] E. Ben-Naim and P. L. Krapivsky, Kinetic theory of random graphs: From paths to cycles, Phys. Rev. E **71**, 026129 (2005).
[41] A. Aharony, Y. Gefen, and A. Kapitulnik, Scaling at the percolation threshold above six dimensions, J. Phys. A **17**, L197 (1984).
[42] M. Lu, S. Fang, Z. Zhou, and Y. Deng (unpublished).
[43] W. Huang, P. Hou, J. Wang, R. M. Ziff, and Y. Deng, Critical percolation clusters in seven dimensions and on a complete graph, Phys. Rev. E **97**, 022107 (2018).
[44] M. Aizenman, On the number of incipient spanning clusters, Nucl. Phys. B **485**, 551 (1997).
[45] S. Fortunato, A. Aharony, A. Coniglio, and D. Stauffer, Number of spanning clusters at the high-dimensional percolation thresholds, Phys. Rev. E **70**, 056116 (2004).
[46] H. W. J. Blöte and E. Luijten, Universality and the five-dimensional Ising model, Europhys. Lett. **38**, 565 (1997).
[47] P. Lundow and K. Markström, The discontinuity of the specific heat for the 5D Ising model, Nucl. Phys. B **895**, 305 (2015).
[48] P. H. Lundow and K. Markström, Complete graph asymptotics for the Ising and random-cluster models on five-dimensional grids with a cyclic boundary, Phys. Rev. E **91**, 022112 (2015).
[49] E. Luijten, *Interaction Range, Universality and the Upper Critical Dimension* (Delft University Press, Delft, 1997).
[50] Z. Li, Z. Zhou, S. Fang, and Y. Deng, Geometric properties of the complete-graph ising model in the loop representation, arXiv:2302.14381 [math-ph].